Genomic signature of shifts in selection in a sub-alpine ant and its physiological adaptations

Cicconardi Francesco[1], Krapf Patrick[2], D'Annessa Ilda[3], Gamisch Alexander[2,4], Wagner Herbert C[2], Nguyen Andrew D[5], Economo Evan P[6], Mikheyev Alexander S[7], Guénard Benoit[8], Grabherr Reingard[9], Arthofer Wolfgang[2], di Marino Daniele[10], Steiner Florian M[2], Schlick-Steiner Birgit C[2]

[1] Department of Zoology, University of Cambridge, Cambridge, UK
[2] Department of Ecology, University of Innsbruck, Innsbruck Austria
[3] Istituto di Chimica del Riconoscimento Molecolare, CNR (ICRM-CNR), Milan, Italy
[4] Department of Biosciences, University of Salzburg, Salzburg, Austria
[5] Department of Entomology and Nematology, University of Florida, USA
[6] Biodiversity & Biocomplexity Unit, Okinawa Institute of Science & Technology, Onna, Japan
[7] Ecology and Evolution Unit, Okinawa Institute of Science & Technology, Onna, Japan
[8] School of Biological Sciences, The University of Hong Kong, Hong Kong, China
[9] Institute of Biotechnology, University of Natural Resources and Life Sciences, Vienna, Austria
[10] Polytechnic University of Marche, Department of Life and Environmental Sciences, Ancona, Italy
Corresponding author: francicco@gmail.com

Abstract

Adaptation to climate can drive variation in diversification rates and species richness. Understanding how organisms adapt to extreme environments can therefore provide insightful case studies for both evolutionary biology and climate-change biology. Here, we take advantage of the vast diversity of lifestyles in ants to identify genomic signatures of adaptation to extreme habitats such as high altitude. We hypothesised two parallel patterns would occur in a genome adapting to an extreme habitat: *i*) strong positive selection on genes related to adaptation and, *ii*) a relaxation of previous purifying selection. We tested this hypothesis by sequencing the high-elevation specialist *Tetramorium alpestre* and four related species. In support of our hypothesis, we recorded a strong shift of selective forces in *T. alpestre*. We further disentangled candidate molecular adaptations in both gene expression and protein-coding sequence that were identified by our genome wide analyses. In particular, we demonstrate that *T. alpestre* has *i*) a derived level of expression for *stv* and other heat-shock proteins in chill shock tests, and *ii*) enzymatic enhancement of Hex-T1, a rate-limiting regulatory enzyme that controls the entry of glucose into the glycolytic pathway. Together, our analyses highlight the adaptive molecular changes that support colonisation of high altitude environments.

Introduction

Adaptation of organisms to climate drives variation in diversification rates and species richness among clades. Their climatic niche influences a species' occurrence in space and time (Soberón 2007) and thus is critically important for both speciation (e.g., ecological speciation through climatic niche divergence) and extinction (e.g., due to climate change). Therefore, understanding how organisms manage thermal adaptation is important in terms of both evolutionary biology and climate-change biology, considering the potential world-wide loss of ecological niches (Lamprecht et al. 2018; Rogora et al. 2018). In this context, high elevations, characterized by a short growing season and low annual minimum and mean temperatures, with high daily fluctuation temperatures (Körner et al. 2011), are an important open-air laboratory to study speciation and adaptation to cold habitats; and compared to the great effort in gene-based studies on cold tolerance of model organisms, a lesser effort has been put towards understanding truly cold-tolerant animals at the genomic level (Clark and Worland 2008; Parker et al. 2018). This is even more evident when considering that among the approximately 600 sequenced insect genomes available today only four belong to species ecologically restricted to high altitudes or Antarctic habitats (Keeling et al. 2013; Kelley et al. 2014; Macdonald et al. 2016; Cicconardi et al. 2017a).

As yet, potential patterns of genomic signatures in organisms adapting to more extreme habitats, such as high elevations, have not been identified and, more generally, there is no theory that predicts the rates of genomic change for extreme habitats. Here, we hypothesise two parallel patterns to occur in a genome adapting to an extreme habitat. On the one hand, strong positive selection on genes related

to adaptation, such as genes involved in metabolic pathways, and on the other hand, a relaxation of previous selecting forces, as the conditions of the previous niche are lacking in the new niche. The latter should lead to a reduced number and/or a different set of genes under purifying selection. Specifically, in the case of high-elevation habitats, some heat-shock proteins (HSPs), necessary for coping with extreme heat, should be under relaxation, because heat resistance is not strongly selected for in the average alpine species. A problem with the hypothesis of these two parallel patterns is that there is no test available for the functional consequences of the loss or gain of a specific gene. There are often many pleiotropic effects for genes that make interpretations difficult, and HSPs, expressed upon exposure to stress or during development and growth, are likely to fall into this category. Therefore, we expect signatures of strong positive selection in metabolic genes, and an increase in the relaxation rates in other genes, without being able to specify which these might be. Identifying such genes will help to set up hypotheses to test in the future. A comparative approach offers the strongest method for testing our hypothesis, by comparing genomes of species closely related to each other, but divergent in terms of adaptation to different environments. However, this approach can be limited by insufficient niche divergence within a group or the number of genomes sequenced. Ants are emerging as a leading system for comparative genomics due to the constantly increasing number of available genomes. This resource offers the opportunity to improve the accuracy of orthology detection (Nygaard et al. 2016), to scan for specific mutations, candidate genes, and patterns of acceleration and relaxation in the ant genomes associated with adaptation to cold habitats.

Ants are key species in the Earth's terrestrial ecosystems. They comprise more than 15,442 described species and display an impressive diversity of lifestyles (Hölldobler and Wilson 1990; Bolton 2018; Seifert 2018). Ants are especially notable among insects for their ecological dominance as predators, scavengers, and indirect herbivores. They compose at least one third of the entire insect biomass (Wilson 1990) and colonise all kinds of habitats, including thermobiologically challenging environments. The formicine ant *Melophorus bagoti*, for instance, is active during the hottest periods of the summer day, when air temperatures at ant height exceed 50 ˚C (Christian and Morton 1992). On the other hand, for example, the myrmicine ant *Tetramorium alpestre* inhabits the montane and subalpine belt of the Central and South European mountain systems, with the Alps as its main distribution area (Wagner et al. 2017; Steiner et al. 2010). This species lives mainly between 1300 and 2300 m above sea level (a.s.l.), forages below the ground, and nests are established in cool grassland under stones, in moss, rootage, and dead wood, especially subalpine and alpine grass mats (Seifert 2018). Since *T. alpestre* belongs to a species complex in which no relation between the ecological niche and worker morphology has been detected, searching for adaptive phenotypical differences outside of morphology, for example physiology, has already been suggested (Wagner et al. 2017). This species is also relevant because, among the 79 Palearctic species of the worldwide distributed genus *Tetramorium* (Bolton 2016), it is one of only two species to form colonies with multiple queens (polygynous colonies), showing intermediate states of aggression and a transition from multicoloniality to supercoloniality (Krapf et al. 2018; Seifert 2018). *Tetramorium alpestre* is thus a

114 system well suited for studying both genomic adaptation to high elevation and socio-
115 behavioural evolution.

116 Here, we tested our hypothesis of both increased diversifying and reduced
117 purifying (relaxing) selection resulting from adaptation to an extreme niche using *T.*
118 *alpestre*. We newly sequenced its genome and those of four related *Tetramorium*
119 species with diverging ecological niches: *T. immigrans*, a species of the *T. caespitum*
120 complex to which *T. alpestre* also belongs to, in sympatry with *T. alpestre*, but
121 distinct in its altitudinal and ecological habitat; *T. parvispinum*, restricted to
122 mountain forest habitats of the Austral-Asian and Indo-Malayan subregions (Liu et
123 al. 2015); and *T. bicarinatum* and *T. simillimum*, invasive generalist species which
124 occur in warmer habitats (Bertelsmeier et al. 2017; Guénard et al. 2017). Our goals
125 were to define the ecological niche of these ant species based on environmental
126 data, and subsequently to perform gene family expansion/contraction and protein-
127 coding scans for signatures of diversifying and relaxing selection. We also annotated
128 the five HSP subfamilies for 19 ant species to test for possible shifts in selection
129 acting on these gene families. Among the signatures of diversifying selection
130 detected, we performed two experiments in *T. alpestre* and its relative, *T.*
131 *immigrans*: we assessed (i) chill-shock triggered gene-expression patterns of *starvin*
132 (*stv*), a Hsp70 modulator, and certain HSPs involved in recovering from extreme cold,
133 and (ii) the temperature dependence of the enzyme activity of Hexokinase type 1
134 (Hex-T1), a rate-limiting and regulatory enzyme that controls the entry of glucose
135 into the glycolytic pathway, one of the most conserved and essential hexokinase
136 isoenzymes (Jayakumar et al. 2007). The genomic data presented here contribute to

a foundation for studying insect genome evolution, particularly also in the light of climate change.

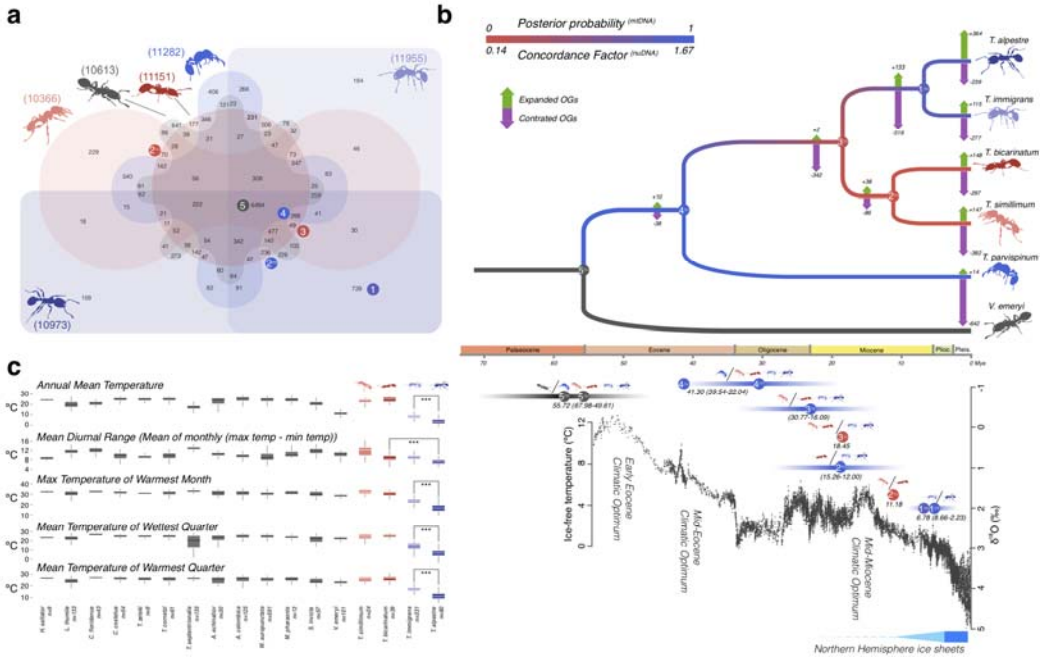

Figure 1. *a*) Venn diagram displaying overlap in orthologous genes in the five *Tetramorium* spp. + *V. emeryi* (Crematogastrini). Coloured circles with number represent phylogenetic splits in the nuDNA (N^{nu}) and mitochondrial phylogenies in *b*; *b*) The dated Crematogastrini nuclear phylogeny (above). Branch colour are based on the concordance factors of the two datasets (nuDNA and mtDNA). On each branch, the numbers of expanded (green arrows) or contracted (purple arrows) genes is shown, inferred from observed OGs sizes at terminal branches. In the bottom, the global $\delta^{18}O$ (‰) derived from analyses of two common and long-lived benthic taxa are given, *Cibicidoides* and *Nuttallides*, which reflect the global deep-sea oxygen and carbon isotope and thus the temperature (from Zachos et al., 2001). Bars represent the 95% confidence interval for the BI analysis, circles with numbers the phylogenetic splits in the nuDNA (N^{nu}) and mtDNA (N^{mt}) phylogenies. *c*) Boxplots of the five bioclimatic variables significantly different for *T. alpestre* and the other ant species.

Results

Climatic niches

A dataset contains 1835 localities representing 17 species was assembled, with the number of localities per species ranging from 9 to 591 (Table S1). Of the 19 bioclimatic variables, four (bio1: Annual Mean Temperature, bio5: Max Temperature of Warmest Month, bio8: Mean Temperature of Wettest Quarter, bio10: Mean Temperature of Warmest Quarter) differentiated between *T. alpestre* and other ants

158 (adjusted *P*-values < 0.001) (Figure 1a). In detail, *T. immigrans* and *T. alpestre* occupy
159 habitats that are colder in the growing season than those of the remaining species,
160 with *T. alpestre* revealing even colder habitats compared with *T. immigrans*.
161
162 **Sequencing, assembly, and annotation of the *Tetramorium* genomes**
163 The combination of overlapping paired-end libraries with very high coverage,
164 standard short paired-end libraries, and mate pair libraries resulted in an overall
165 complete assembly of the five *de novo Tetramorium* genomes, at the level of both
166 contiguity and scaffolding. In particular, the *T. alpestre* genome contiguity (contig
167 N50) is the 3rd best among all ant genomes available (Table S2). The analysis of the *k*-
168 mer frequency distribution generated was unimodal (Figure S1; Supplementary
169 Material online), and an analysis of the distribution of GC content across the five *de*
170 *novo Tetramorium* genomes revealed similar distributions with a mean of 38%, that
171 is, slightly less than that found in *V. emeryi* (42%) (Figure S2). No significant bias was
172 recovered considering GC content and coverage (Figure S3). All five *de novo* draft
173 assemblies were ~241 Mb in length, comparable in size with the average of all ant
174 genomes available (~278 Mb) (Table S2). The total *T. alpestre* genome size was
175 245.72 Mb, including 18 Mb of gaps and unknown characters (N/X), slightly smaller
176 than the estimated genome size by flow-cytometry of 291.84 Mb +/- 1.76 Mb (n=12).
177 Repetitive elements made up similar proportions of each sequenced genome (*T.*
178 *alpestre* = 18%, *T. immigrans* = 20%, *T. bicarinatum* = 21%, *T. simillimum* = 20%,
179 *T. parvispinum* = 23%; Table S2), indicating a strong correlation between genome
180 size and total interspersed repeat content (Pearson ρ = 0.976, *P*-value < 0.005; Figure
181 S5). For the gene annotations in *T. alpestre*, a combinatorial approach of

unsupervised RNA-seq-based, homology-based, *ab initio*, and finally *de novo* methods were used. By doing so, we approached the number of predicted protein-coding genes in the phylogenetically closest annotated species (15,085 genes predicted vs. 14,872 in the *V. emeryi* genome, Table S2). This improved the homology-based annotation of the remaining four *Tetramorium* genome assemblies that did not differ much in terms of estimated gene content, ranging from 16k to 15k annotated loci (Table S2). BUSCO analyses estimated overall good representation, with recovered genes in between the 97.6% and 99.9% (Table S2; Figure S6), and all statistics on mRNA, coding regions (CDS), exon, and intron length gave highly similar and overlapping distributions among all *Tetramorium* species and *D. melanogaster* as a reference (Figure S7). Also, the transcript completeness gave good results with a comparable distribution of percentage of alignment across species (Figure S8).

The orthology search analysis produced a total of 7195 OGs between *D. melanogaster* and Hymenoptera; 3261 of these represented scOGs present in all 22 species analysed. Restricting the orthology analysis to *Tetramorium* spp. and *V. emeryi* resulted in 6494 OGs; among *Tetramorium*, the highest fraction was recovered between *T. alpestre* and *T. immigrans* with 729 OGs, followed by *T. simillimum* and *T. parvispinum* (540 OGs) (Figure 1a). For all *Tetramorium* species., the fraction of orthologous genes with at least a match with one of the three outgroups (*A. mellifera, N. vitripennis, D. melanogaster*) was on average 7286, with the highest in *T. alpestre* (7879) and the lowest in *T. parvispinum* (6977), in line with the average value found in ants (7831).

Assembly and annotation of ant mitogenomes and their gene translocations

We assembled complete mtDNA genome sequences from 24 ant species. Because of the differences among SRA datasets, we used different numbers of reads to assemble the complete sequences. The new mtDNA genomes were slightly longer (on average, 17k vs. 16k; Table S2), probably due to the reconstruction of the D-loop and ribosomal genes, which are sometimes harder to assemble. We slightly mis-assembled a coding gene (*nad2*) in the *T. bicarinatum* genome and a few other tRNA loci in other genomes (Table S2). The average GC-content for coding genes was 23.9 ± 3.0% and varied slightly among taxa with the lowest in *Formica fusca* (19.0%) and the highest in *Leptomyrmex pallens* (32.8%) (Table S2). While almost all species had the typical gene order and orientation, some rearrangements were observed. All myrmicine ants were characterized by a translocation of *trnV* after *rrnS*; *Solenopsis* spp. had a swapped position of *rrnS* and *trnN*; *Monomorium pharaonis* had at least three rearrangements: the inversion of *nad6*, *cob*, and *trnS2*, the translocation of *trnE* upstream to *trnA*, and the translocation of *trnR* upstream to *trnE*; *Tetramorium* spp. underwent a swap of *trnR* and *trnN* (Figure S9).

Phylogenetic analyses of *Tetramorium* spp., their diversification dating, and the Miocene-Pliocene origin of the lineage leading to *T. alpestre*

The estimated divergence ages from both datasets (mtDNA, nuDNA) were congruent for most nodes, except for recent nodes within the Attini (Figure 1b; Figure S10-13). In this case, the penalized likelihood approach estimates were always more recent than the estimations made with BI using BEAST. The dating of basal nodes like the MRCAs (e.g., Crematogastrini, Myrmicinae, and Formicinae) were congruent with a previous analysis based on more taxa but fewer genes (Moreau and Bell 2013). The

two methods also converged regarding the date of the most recent common ancestor (MRCA) between *T. alpestre* and *T. immigrans*. In that specific case, PL dated that split at 6.8 million years ago (mya) within the confidence interval given by BI (Median: 5.15 mya; 95% HPD: 2.66, 8.23).

The phylogenetic relationships were generally highly congruent and with predominantly strong support (Figure 1b and Figures S10-13). In the ML phylogeny of scOGs (nuDNA), all nodes were supported with a bootstrap value of 1. Across the whole phylogeny, only a few nodes had weak signals, resulting in very few topological disagreements and low coalescent units (CU). Within the clade of Crematogastrini (*Tetramorium* spp. + *V. emeryi*), the relation of *T. bicarinatum* and *T. simillimum* was uncertain: nuDNA phylogeny recovered them as sister species with low CU (0.11), while mtDNA phylogeny placed *T. bicarinatum* as sister to the *T. alpestre*-*T. immigrans* cluster, with a bootstrap value of 0.77 and a posterior probability of 0.99.

Contractions of OGs in the *T. immigrans* and *T. alpestre* lineages and expansion of retrotransposon-related genes in *T. alpestre*

We examined the evolutionary dynamics of OGs looking at more dynamic ranges corresponding with terminal branches. We observed an increased number of OG deaths in the *T. parvispinum* lineage (– 642) and in the lineage leading to *T. alpestre* and *T. immigrans* (– 516). Ortholog groups showed very little expansion in internal branches of the *Tetramorium* radiation. Expanded OGs were common in terminal branches, except for *T. parvispinum* with very few expanded OGs (+ 14), suggesting a possible lack of annotation. *Tetramorium alpestre* showed the highest number of

expanded OGs (+ 364) (Figure 1b), with more than 370 of them (~ 40%) belonging to genes with reverse transcriptase (PFAM: rve, rve_1, rve_2) or transposase and retrotransposon activities (PFAM: Retrotrans_gag, Retrotran_gag_2). Among other PFAM, haemolymph juvenile hormone-binding proteins (PFAM: JHBP; 20 genes), zinc fingers (PFAM: zf-CCHC, zf-H2C2, zf-met, 32 genes), and sugar transporters (PFAM: Sugar_tr, 4 genes) were found.

Dual signature of evolutionary pressures in single-copy OGs in the *T. alpestre* genome

We investigated the impact of evolutionary pressures on one-to-one orthology in the five *Tetramorium* spp. and 14 other ant species and three outgroups (*Apis mellifera*, *Nasonia vitripennis*, and *Drosophila melanogaster*) by computing both mean ω (d_N/d_S) for terminal branches and relaxing selection (k) within the Crematogastrini.

The measure of the mean branch ω showed an overall high level of purifying selection along the whole ant phylogeny, including for short branches (Roux et al. 2014; Cicconardi et al. 2017b), with median values of 0.10. However, this distribution was significantly shifted in *T. alpestre*, which showed a median value of 0.38 (Wilcoxon rank-sum test '*greater*', *P*-value < $2.2e^{-16}$), whilst keeping the proportion of $\omega > 1$ in each branch unchanged (Figure 2a, S13). The evaluation of k in the five *Tetramorium* spp. and *V. emeryi* had a mean of median values of 0.99, that is, twice the value in *T. alpestre* (median $k = 0.47$; Wilcoxon rank-sum test '*less*', *P*-value < $2.2e^{-16}$) (Figure 2b). We investigated the nature of the increased ω (episodic diversifying selection) and decreased k (relaxed selection) in *T. alpestre* by combining the two measures. Two evolutionary trajectories appeared to act simultaneously

(two tails of the distribution, Figure 2c): One trajectory seems to have led to episodic diversifying selection,

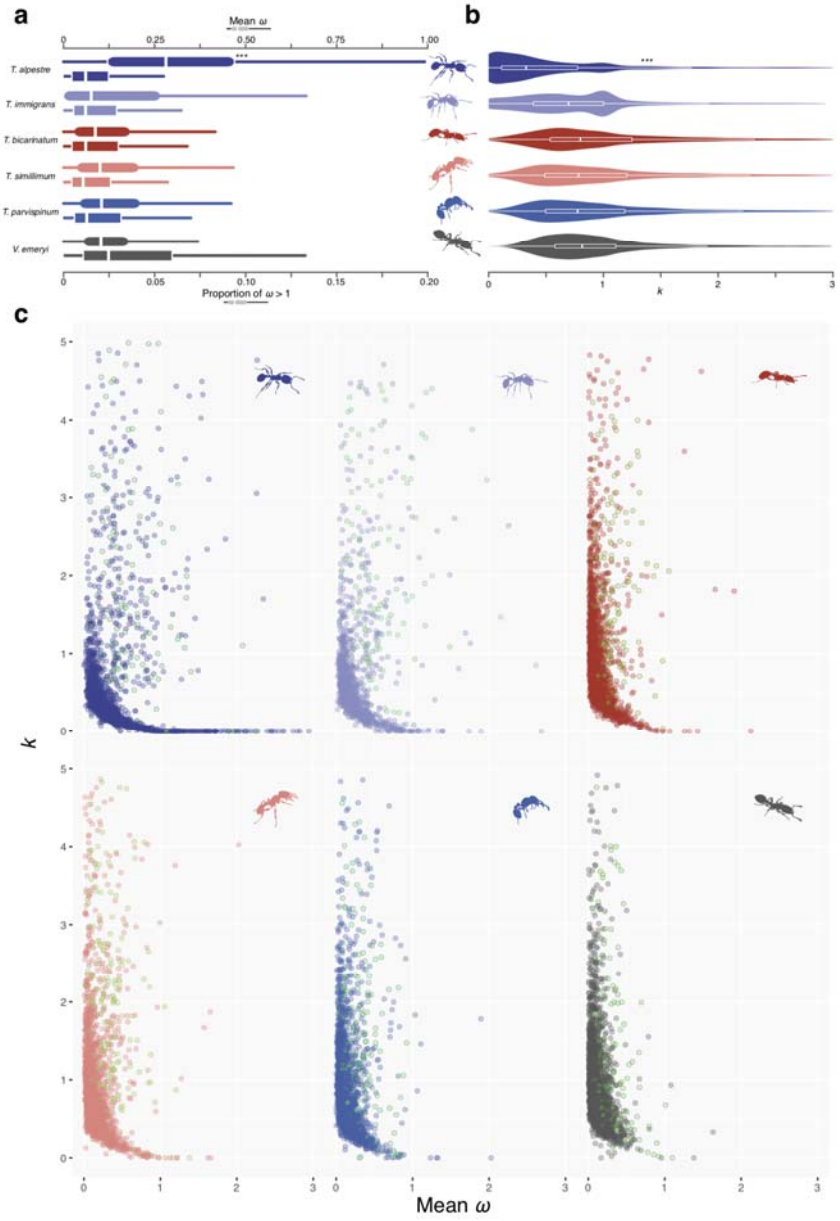

Figure2. *a*) Boxplots showing the distribution and median (vertical line) of mean ω (d_N/d_S) rates (square shapes) in terminal branches of *Tetramorium* spp. and *V. emeryi* (Crematogastrini) in scOGs, and the proportion of genes for which ω is higher than one. *b*) Boxplots overlapped by violin plots showing the distribution of k in Crematogastrini. The distribution in *T. alpestre* is clearly bimodal as in *T. immigrans*, but with a much more skewed distribution towards zero values. In both sections, asterisks indicate the degree of significance between *T. alpestre* and the other species (Wilcoxon rank-sum tests). *c*) Scatter plots for each Crematogastrini species included, showing for each scOG branch both values of ω and k. The green dots are scOGs with uncorrected *P*-values associated with diversifying selection less than 0.05. The distribution in *T. alpestre* shows the longest tail

corresponding to very low values of k and high values of ω. It is also notable a much wider and scattered distribution of scOGs with high k and ω compared with all other species.

promoting the fixation of nonsynonymous mutations with presumably advantageous fitness effects for genes with increased values of ω and k, also present in the other species. The other trajectory showed a relaxation of the overall purifying selection in genes with increased values of ω and decreased values of k, only mildly present in *T. immigrans*.

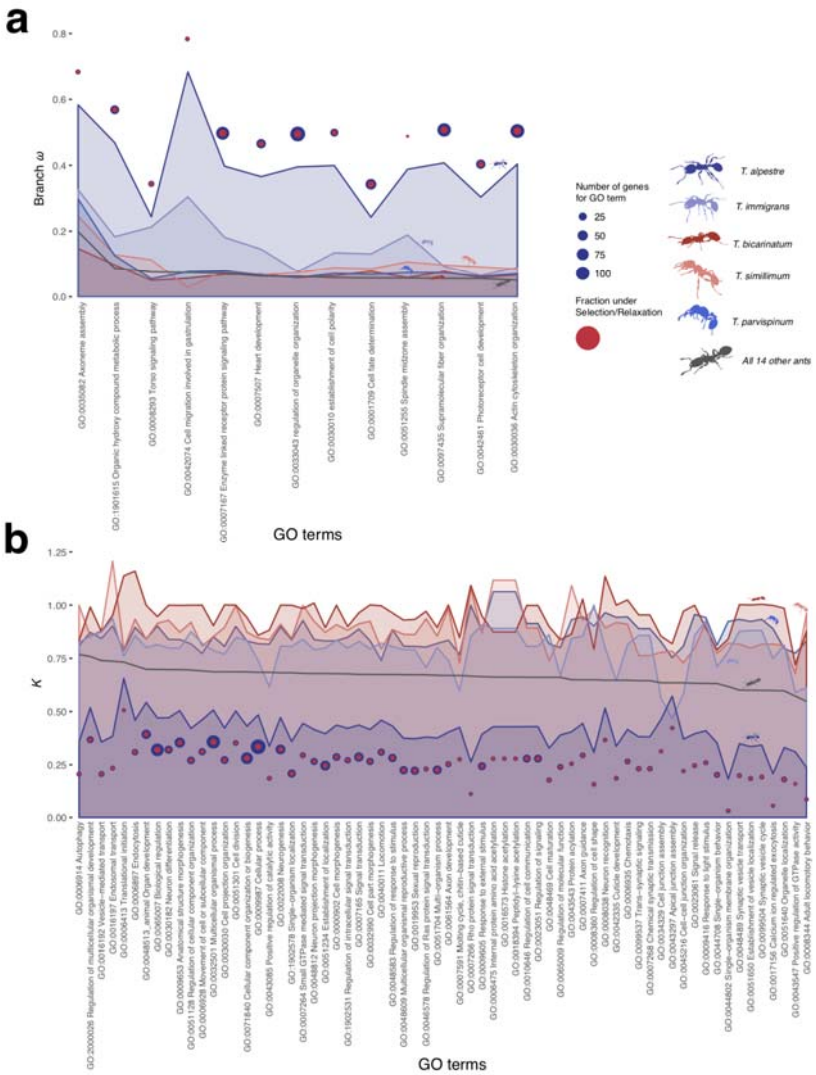

Figure 3. For each enriched Gene Ontology (GO) term category *a*) the median values of ω; and *b*) k for genes enriching the specific category. *Tetramorium* spp. are colour coded, the other 14 species, merged to obtain a background signal, are in gray. Blue circles are scOGs tested for each GO term, red circles are scOGs returned as significant. Circle sizes are proportional to the number of genes. To be noted are the overall extremely higher

values of ω and lower values of k in *T. alpestre* branches compared to the other species. Seldomly also *T. immigrans* shows few GO terms with high ω and low k values, in particular the Apical junction assembly (GO:0043297) shows and inverted trend between *T. alpestre* and *T. immigrans*.

After a stringent correction for multiple testing, we found 175 scOGs with a putative signature of diversifying selection (adjusted *P*-values < 0.005; Table S5), with 50 genes enriching 13 biological process terms (*P*-values < 0.005; Figure 3a, Table S6), nine related to cell development (e.g., cell migration involved in gastrulation, photoreceptor cell development, cell fate determination) and organization (e.g., regulation of organelle organization), two related to signalling pathways (enzyme linked receptor protein signalling pathway and torso signalling pathway), one to heart development, and one to organic hydroxy-compound metabolic processes. The most representative genes were *Pten* and *Gbeta13F*, involved in six biological processes, *DCTN1-p150* and *dsh*, involved in five of them. All key genes are involved in the proliferation and division of cells, especially neurological stem cells (*Gbeta13F*), respiratory system development (*Pten* and *dsh*), and the serine/threonine-protein kinase *polo*, present in four enriched Gene Ontology (GO) terms. In the catalytic domain of this protein (255 aa), we found five amino acid substitutions compared with *T. immigrans*, three of them corresponding to active sites ($TalpPolo_{G29V}$, $TalpPolo_{G30R}$, $TalpPolo_{S104R}$). We also tested for possible enrichment in KEGG pathways and found three significant pathways (*P*-values < 0.02; Table S7), all involved in the metabolic processes of galactose metabolism and the glycolysis pathway, the pentose phosphate pathway, and galactose metabolism, with five enzymes under diversifying selection: a glucose-6-phosphate (*CG9008*), the hexokinase type 1 (*Hex-T1*), a phosphofructokinase (*Pfk*), a transketolase (*CG8036*), and a phosphoglucosemutase (*pgm*).

132 scOGs had a signature of putative relaxation (*P*-values < 0.005; Table S8). While the absolute number of scOGs under relaxation was slightly lower than the number of genes under diversifying selection, the gene-set enrichment tests revealed many more biological processes significantly enriched: 70 terms (*P*-values < 0.005; Figure 3b, Table S9) enriched by 118 genes. Fifteen terms were related to the regulation of cellular development, signal transduction, and cell communication (e.g., regulation of response to stimuli, regulation of cell communication, regulation of Ras signal transduction), 12 terms related to neurogenesis, axon development, and synaptic transmission (e.g., neuron differentiation, trans-synaptic signalling, axon guidance), seven terms were related to cell morphogenesis and junction organization, and many other related to response to stimuli (e.g., chemotaxis, response to light) or related to adult development and morphogenesis (e.g., anatomical structure morphogenesis, molting cycle, chitin-based cuticle). The enrichment of KEGG pathways revealed three pathways: mRNA surveillance pathway, spliceosome, and protein processing in endoplasmic reticulum (*P*-values < 0.05; Table S10).

The Hex-T1 activity, its model structure, and molecular dynamics simulations in *T. alpestre* and *T. immigrans*

As we describe in the previous section, the enrichment for KEGG pathways led to the identification of three metabolic pathways, all involved in the metabolism of sugars, with five genes under selection. We therefore aimed at the experimental validation of their functionalities comparing their activity in *T. alpestre* and the most closely related species in this dataset, *T. immigrans*. We tried to assay the four enzymes, but

unfortunately, we were able to correctly synthesise only Hex-T1. The assay was designed to measure the efficiency of Hex-T1 in both species and in a temperature gradient, at 6, 16, 26, and 36 °C. The assays showed that the Km value was always

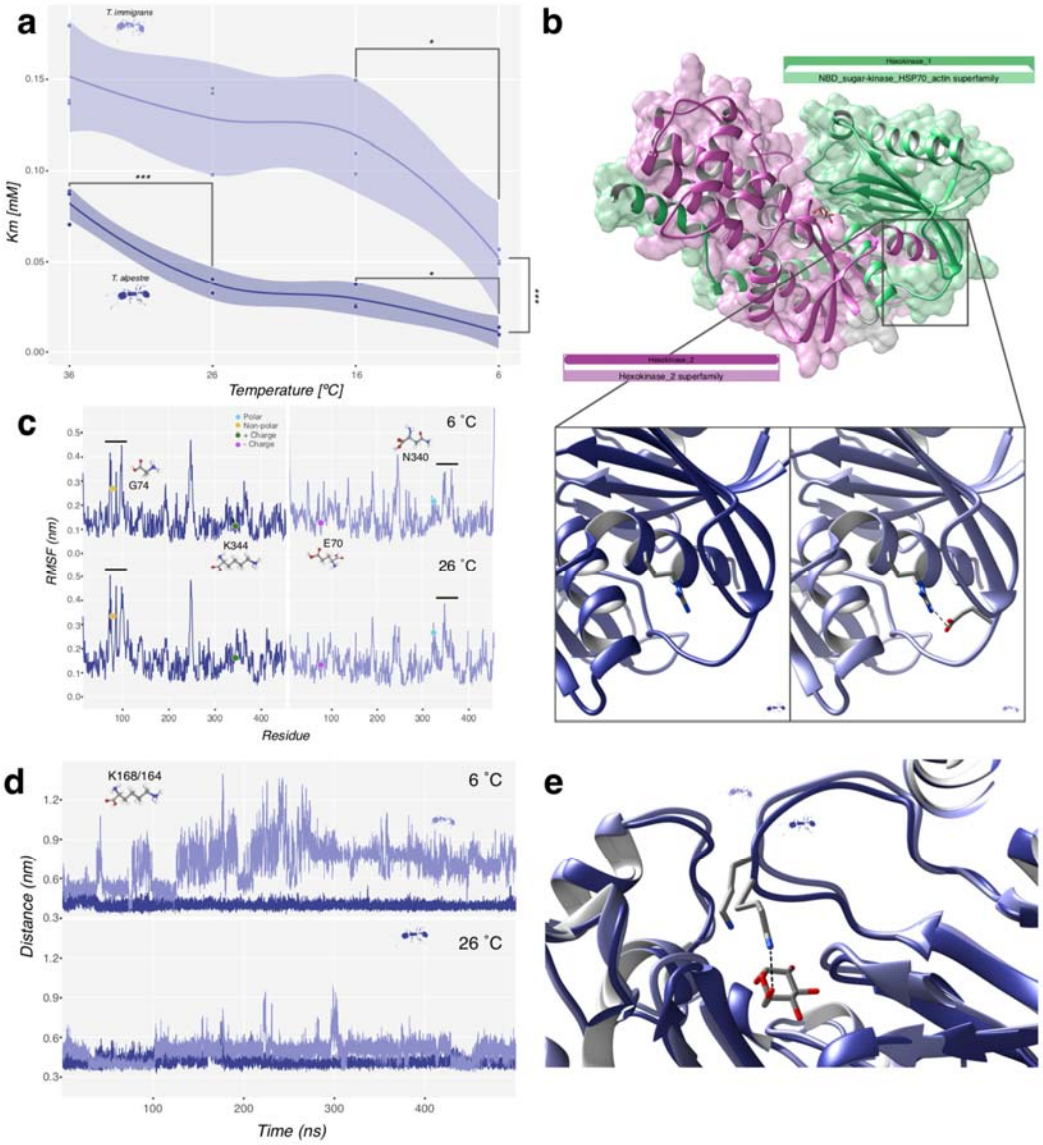

Figure 4. *a*) Scatter plot of Km score across the temperature gradient in the two species, *T. immigrans* on top and *T. alpestre* on the bottom. Lines represent average values with confidence intervals. Significances: *** < 0.001; ** < 0.001; * < 0.05. *b*) Overview of the homology-modeled structure of Hex-T1 in *T. alpestre* showing the two Hexokinase domains, PFAM00349 (green) and PFAM03727 (pink). The lower panels show the location of TalpHex-T1$_{G74}$ (left) and TimmHex-T1$_{E70}$ (right) as well as the arginine residue that forms a salt bridge with E70 (dashed line). *c*) Per-Residue Root Mean Square Fluctuation (RMSF) calculated along 500 ns trajectories carried out at 6 °C (upper panel) and 26 °C (lower panel) for TalpHex-T1 (left panel, blue line) and TimmHex-T1 (right panel, light blue line). The location of the residues found mutated between the two sequences are indicated. *d*) Time evolution of the atomic distance between the centre of mass of glucose and the lateral chain nitrogen atom of TalpHex-T1$_{K168}$ (blue line) and TimmHex-T1$_{K164}$ (light blue line) in the binding pocket calculated along the 500 ns trajectories carried out at 6 °C (upper panel) and 26 °C (lower panel). *e*) Representative configurations extracted

366 from the simulations at 26 °C showing the different orientation of TalpHex-T1$_{K168}$ and TimmHex-T1$_{K164}$, with the
367 first one being the only one able to bind the glucose (dashed line).
368

369 lower in *T. alpestre* than in *T. immigrans* (Wilcoxon rank-sum test 'less', *P*-value <
370 0.00004, Figure 4a), with values ranging from 0.08 mM to 0.01 mM in *T. alpestre*
371 versus 0.15 mM to 0.05 mM in *T. immigrans*, from the highest to the lowest
372 temperature; reflecting that less substrate concentration was needed for the *T.*
373 *alpestre* enzyme to reach half of its maximal reaction speed, that is, Hex-T1 of *T.*
374 *alpestre* was always more efficient than of *T. immigrans*. Although the number of
375 replicates per condition was small, we performed statistical tests to attempt
376 obtaining insight in the enzymatic activity differences within species at different
377 temperatures and in their variance. Interestingly, it seems that for both species
378 there is an improvement in the Km values shifting towards the lowest temperatures
379 (6 °C *vs* 16 °C; two-way ANOVA followed by a Tukey's multiple comparison; adjusted
380 *P*-values < 0.05), and a possible deterioration at higher temperatures in *T. alpestre*,
381 from 0.04±0.01 mM (26 °C) to 0.08±0.01 mM (36 °C) (two-way ANOVA followed by a
382 Tukey's multiple comparison; adjusted *P*-value < 0.0002). An F test (VAR.TEST()
383 implemented in R) to compare the variances of the enzymatic activities (Km values)
384 between the two species – by pooling the replicates at 16 and 26 °C – suggested that
385 there is a possible significant difference in their variance (*P*-value = 0.015), with the
386 confidence interval of Hex-T1 activity in *T. immigrans* twice wider as in *T. alpestre*.

387 The Hex-T1 enzyme is made of two structurally similar domains, Hexokinase 1
388 and 2 (PFAM00349 and PFAM03727), and an N-terminus that is highly variable both in
389 terms of length and amino acidic composition (Figure 4b). The two domains are
390 relatively well conserved across all ants, other Hymenoptera and *D. melanogaster*.

Excluding the hypervariable N-terminus, and considering the two functional domains, the amino acid sequences of *T. alpestre* and *T. immigrans* only differ by two amino-acidic changes: a glutamic acid (E) replaced by a glycine (G) in position 74 (TalpHex-T1$_{E74G}$) (Figure 4b inserts) and an asparagine (N) replaced by a lysine (K) in position 344 (TalpHex-T1$_{N344K}$). While the second change probably does not entail a significant functionality effect, the *TalpHex-T1$_{E74G}$* instead may be significant. Because of the lack of the long chain and the negative charge, this modification could give the protein a higher flexibility and therefore an overall higher kinetics. We tested this hypothesis by simulating the protein dynamics in the presence of the glucose substrate at different temperatures, i.e. 6 and 26 °C, with the intent of mirroring the condition in the in vitro assay. In the simulations we can see a dual effect. For TalpHex-T1$_{N344K}$, located at the C-terminal of an α-helix forming a helix-turn-helix motif (VSETE**K**DPKG), the Root Mean Square Fluctuation (RMSF) revealed a lower degree of fluctuation in TalpHex-T1 (Figure 4c). This is possibly due to the alternation of positive and negative charges creates a salt-bridges network that stabilizes the whole motif (data not shown). In particular TalpHex-T1$_{K344}$ is involved in a stable interaction with TalpHex-T1$_{E341}$ (data not shown), while TimmHex-T1$_{N340}$ is not available for the formation of salt bridges and mainly establishes hydrogen bonds with TimmHex-T1$_{S336}$ or TimmHex-T1$_{E337}$ at 6 or 26 °C, respectively. Although the *T. alpestre* salt bridge brings a higher flexibility of the helix-turn-helix motive, it does not interfere with the catalytic site, given that this motif is far away in the C-terminal region of the protein.

In contrast, at the other region (TalpHex-T1$_{E74G}$), the mutation-caused amino acid change allows the loop to explore a broader conformational space equipping it

415 with a higher degree of flexibility already at 6 °C (Figure 4c). Nevertheless, by
416 increasing the temperature, TalpHex-T1 was subjected to an even higher degree of
417 fluctuation, once again confirming the intrinsic flexibility led by the glycine. Notably,
418 the increased flexibility is also transferred to residues relatively far from the
419 mutation, in particular in regions near the active site (168-169), causing a different
420 pattern of interaction with the substrate (Figure 4d, e). Indeed, TalpHex-T1
421 established a stronger interaction with glucose at both temperatures with respect to
422 TimmHex-T1 (Figure 4e).
423
424 **The heat-shock proteins in ants and their evolution in *T. alpestre***
425 Members of the five subfamilies of the heat shock proteins (HSPs: Hsp90s, Hsp70s,
426 Hsp60s, Hsp40s, and sHsps) were fully recovered and characterized in 19 ant species.
427 Overall, a strong purifying selection was observed within subfamilies (Figure 5a,
428 Table S11). In the Hsp90 gene family (*trap1*, *gp93*, and *Hsp83*) *Hsp83* was found
429 duplicated within the lineage of *W. auropunctata* (inparalog), as well as the *T.*
430 *parvispinum gp93*; duplication that probably occurred before emergence of the
431 lineage (outparalog) (Figure S14). Members of the Hsp70 family were recovered for
432 all species with 11 ortholog groups, with few duplications in *Hsc70-3* and *Hsc70-5*
433 (two inparalogs and two outparalogs, respectively). We confirmed the lack of Hsp70s
434 in ants (Nguyen et al. 2016) and a multiple duplication of *Hsc70-4* in Hymenoptera.
435 One paralog seemed to be lost in many species while the other two copies were still
436 present in almost all species, with the presence of other outparalogs in various
437 species, mostly in Attini (Figure S15). The chaperonin Cpn60/TCP-1 family (Hsp60)
438 had nine OGs; six inparalogs were found in *CCT7, CCT3* and four outparalogs in

439 *Tcp1a*, *CCT8*. The heat shock protein 40 kDa/Chaperone DnaJ was the largest
440 subfamily, with 37 well-defined OGs. Its turnover of duplication was relatively small,
441 and only six OGs showed some level of duplication. The small HSPs (sHsps) showed
442 the expansion of the lethal (2) essential for life (*l(2)efl*) gene paralog of *D.*
443 *melanogaster*, with five distinct OGs in all Hymenoptera. *L(2)efl3* seemed to be
444 retained by only in 11 species, and with *l(2)efl4*, they are the two most divergent
445 OGs, with ω equal to 0.23 and 0.33, respectively. The less divergent were *Hspb1* and
446 *l(2)efl5*, for which ω was 0.11 and 0.07, respectively. Overall, the sHsps showed a
447 significantly higher distribution of ω (median = 0.22, *P*-value = 0.013), followed by
448 Hsp40s, which also showed a wide distribution of ω. In contrast, Hsp90s, Hsp70s,
449 and Hsp60s seemed to be very stable and under a very high purifying selection.

450 To understand other possible mechanisms of adaptation of *T. alpestre* to the
451 cold, we computed the mean values of ω and k for all branches leading to
452 *Tetramorium* spp. and *V. emeryi*, integrating 13 ant species, and scanned for
453 diversifying and relaxed selection specifically in *T. alpestre*. The first part of the
454 analysis showed a similar landscape as observed in scOGs. Among the five
455 *Tetramorium* species and *V. emeryi*, five species display a distribution of the mean-
456 branch ω ranging between 0.07 (*T. immigrans*) and 0.13 (*T. parvispinum*); *T. alpestre*
457 instead showed significant 2.7-fold higher value of the median mean-branch ω (ω =
458 0.36, Wilcoxon rank-sum test '*greater*', adjusted *P*-values < 0.004, Figure 5b). The
459 distribution of k among HSPs in the six species showed median values of k all close to
460 the expected (k = 1), between 0.90 in *V. emeryi* and 1.05 in *T. simillimum*, again with
461 the exception of *T. alpestre*, where the median k = 0.63, 1.4-fold lower than the
462 lowest median k (Wilcoxon rank-sum test '*less*', adjusted *P*-values < 0.05, Figure 5c).

463 The scan for diversifying positive and relaxed selection in branches of the HSPs of *T.*

464 *alpestre*

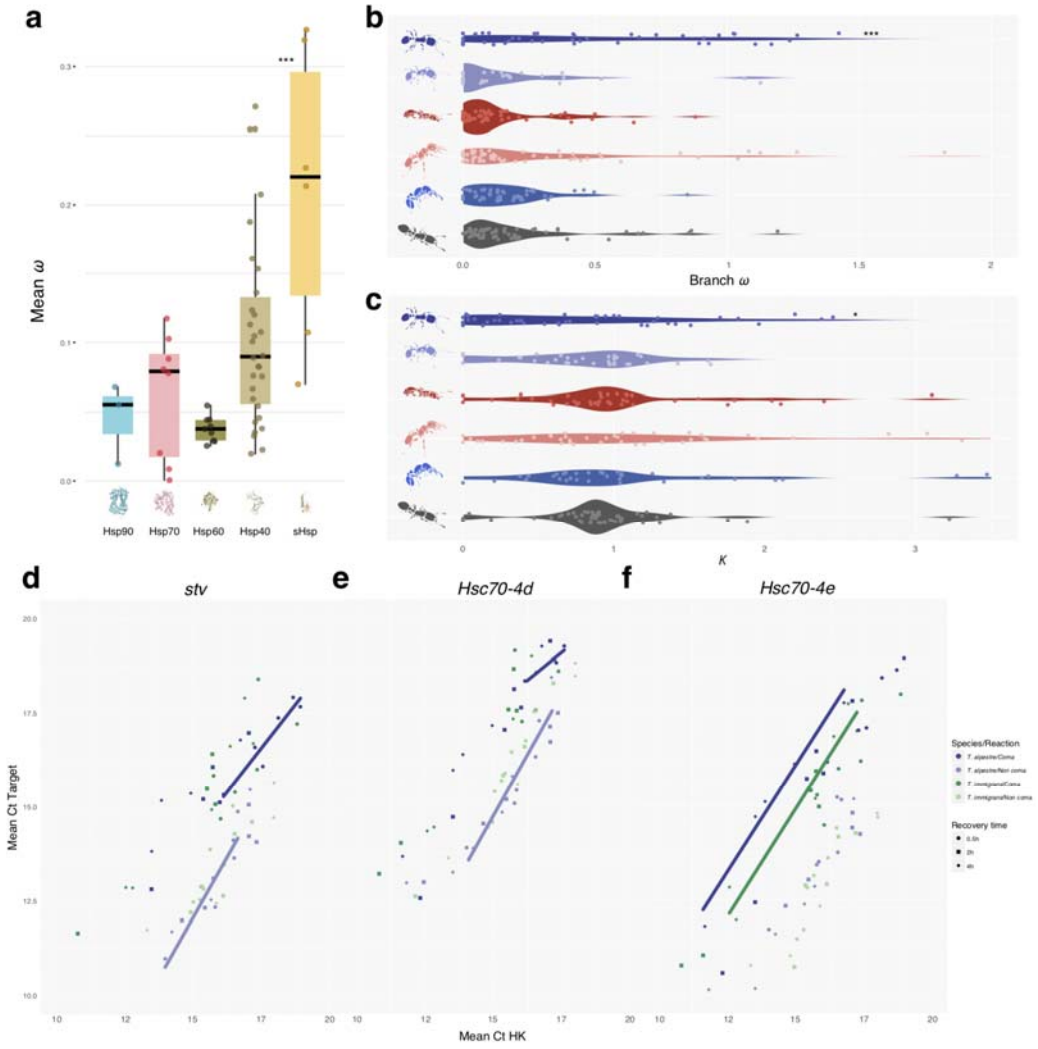

465

466 ***Figure 5.*** *a*) Boxplots showing the distribution and median (horizontal black line) of mean ω (d_N/d_S) rates for each
467 of the HSP subfamily. *b*) Violin plot showing the distribution of the mean ω values; and *c*) *k* in the terminal
468 branches of the Crematogastrini (from up to bottom: *T. alpestre*, *T. immigrans*, *T. bicarinatum*, *T. simillimum*, *T.*
469 *parvispinum*, *V. emeryi*). *d-f*) Scatter plot of target gene (*stv*, *Hsc70-4d*, *Hsc70-4e*) vs. housekeeping gene (HK)
470 concentrations; concentrations given as total number of cycles minus cycle threshold (Ct) values, that is, higher
471 values represent higher concentrations. Straight lines are linear regressions for each target gene against HK using
472 the different recovery times separately; based on one-way analysis of covariance followed by correction for
473 multiple comparison, just lines for those treatment / recovery-time combinations are shown for which
474 significances for just a single species arose, that is, *T. alpestre* coma vs. non-coma after 0.5 h (*d, e*; no difference
475 in *T. immigrans*) or for which the two species differed, that is, *T. alpestre* coma vs *T. immigrans* coma after 4.0 h
476 (*f*).
477

478 showed no gene under putative diversifying positive selection, while six loci were
479 identified to be under putative relaxing selection: one Hsp90 (*Trap1*), two Hsp60
480 (*CCT4*, *CCT5*), and three Hsp40s (*Sec63*, *DnajC8*, *DnajC11*) ($k < 0.14$, adjusted *P*-values
481 < 0.005). Using these genes in prediction interaction networks, we found that the
482 two Hsp60s interacted with other 21 genes, giving 17 significant enriched functions
483 (FDR < 0.05), mainly related to protein folding and microtubule, spindle organization;
484 the three Hsp40s interacted with 21 genes, giving two enriched functions (FDR <
485 0.05), related to response to heat and response to temperature stimulus (Figure
486 S19).
487
488 **Chill shock effect, recovery times, and expression patterns of *stv* and HSPs in *T.***
489 ***alpestre* and *T. immigrans***
490 Among the genes with a putative signature of diversifying selection, we also found
491 *starvin* (*stv*), a BAG-family member which seems to be implicated in Hsp70 ATPase
492 activity during cold recovery in *D. melanogaster* (Colinet and Hoffmann 2010).
493 Therefore, we explored if the modulation of its expression may play a role in how *T.*
494 *alpestre* differently withstands the cold compared to the related species *T.*
495 *immigrans*. We thus performed a pilot test measuring the different expression
496 patterns of *stv*, two paralogs of *D. melanogaster Hsc70-4* (*Hsc70-4d* and *Hsc70-4e*), a
497 member of the Hsp90 subfamily (*Hsp83*), and sHsp *l(2)efl4* in the two species.
498 We measured the transcription activity of three recovery times (0.5 h, 2.0 h,
499 and 4.0 h) and compared coma and non-coma individuals and found a significant
500 difference in the expression patterns of *stv*, *Hsc70-4d*, *Hsc70-4e*, and *Hsp83*, but not
501 of *l(2)efl4* (one-way ANCOVA followed by Bonferroni-Holm correction). In particular,

looking at the different recovery times, *stv* and *Hsc70-4d* responded quickly in *T. alpestre* but not in *T. immigrans,* being significantly expressed only in workers of *T. alpestre* after 0.5 h recovery, but not in *T. immigrans* (Figure 5d-e). Comparing the expression levels between species, we found higher mRNA levels for *Hsc70-4e* in *T. alpestre* after 4 h recovery (Figure 5f).

Discussion

Tetramorium alpestre represents a critical example of evolutionary adaptation to cold environments such as alpine habitats, characterized by low temperatures during the growing season (Figure 1c). By analyzing its genome in the context of 18 other ant species, we shed new light on the evolution and adaptation of this ant, which can serve as a potential model for arthropod adaptation to cold habitats. We found good concordance between the nuclear and the mitochondrial dated phylogenies, concerning the dating of the speciation of *T. alpestre*, which seems to have diverged from its closest relative, *T. immigrans*, between 2 and 9 mya. This period overlaps with the beginning of a new climatic zonation of the European continent during the Middle and earliest Late Miocene (Zachos et al. 2001). At the end of this period, a rapid uplift (~5 mya) fundamentally changed the paleogeographic and topographic setting of central and southern Europe and triggered Alpine glaciation (Kuhlemann 2007). Interestingly, both paleoclimatic and paleogeographic changes co-occurred with the origin of the lineage leading to *T. alpestre* (Figure 1b). In fact, while these glaciations dramatically reshaped global biodiversity patterns, eliminating terrestrial biota from many mid- to high-latitude areas, they may have been the main driver of

526 diversification on highlands by reducing gene flow among populations (Wallis et al.
527 2016).

528 The present results support our prediction that two parallel patterns will
529 occur in the genome of species adapting to extreme habitats. The genome of *T.*
530 *alpestre* appears to be under the influence of two strong evolutionary trajectories:
531 on the one hand, a diversifying selective force, two-fold higher compared with all
532 other ants, and on the other hand, a relaxation of the overall purifying selection
533 present in other ants, identified by the skewed distribution of k towards zero.
534 Specifically, the diversifying selective force affects more than a hundred genes in
535 many key biological processes, such as those related to development, cell migration,
536 and gastrulation. Genes under the category of biological processes are also under
537 selection in the genome of the Antarctic midge *Belgica antarctica* (Kelley et al. 2014).
538 In fact, early stages are the most fragile ones, having the highest rate of lethal
539 phenotypes during heat shock and UV irradiation, particularly around gastrulation
540 (Uchida et al. 2018). The same may pertain to genes related to cellular-level
541 organization (e.g., spindle midzone assembly, supramolecular fiber organization,
542 actin cytoskeleton organization), where environmental stress may jeopardise a well
543 working cell division machinery, as SNPs associated to long-term cold-adaptation
544 plasticity were found to be present in genes related to cytoskeletal and membrane
545 structural components in *D. melanogaster* (Gerken et al. 2015). Among 25 genes
546 involved in these biological processes, *polo*, a polo-like kinase which plays a central
547 role as regulator of cell division and is required for several events of mitosis and
548 cytokinesis (Archambault et al. 2015), shows three amino acid substitutions in

549 positions corresponding to active binding sites, and thus could be a good candidate
550 for further studies.

551 The two evolutionary trajectories were predicted in our hypothesis, and while
552 diversifying selection is somewhat expected in species adapting to a new
553 environmental niche, the magnitude of relaxed selection found is more surprising
554 and never recorded. Although both ω and k distributions in *T. alpestre* are highly
555 skewed, the absolute number of genes under diversifying and relaxed selection are
556 not markedly greater than other species in similar studies (Cicconardi et al. 2017b;
557 Roux et al. 2014; Harpur et al. 2014). This cannot be directly ascribed to the type *I*
558 error rate because the same rate should be equally randomly present in all the other
559 short or long branches of the phylogeny. Nevertheless, *T. alpestre*, as part of a
560 species complex (Steiner et al. 2010; Wagner et al. 2017), may have more recently
561 diverged from more closely related species not yet adapted to the alpine habitat.
562 Magnitude of this relaxed selection is evidenced by the 70 enriched biological
563 processes, and can be possibly seen as the consequence of a shift and/or decreased
564 magnitude in the purifying selection. The direct implication of this relaxation is not
565 clear, especially its effect on genes and their biological processes, such as the
566 regulation of cellular development, signal transduction, cell communication,
567 neurogenesis, axon development, and many others. If the physiology of cold
568 adaptation utilises different metabolic and developmental strategies to minimise
569 and optimise energy consumption, a new balance needs to be reached. The two
570 patterns observed in present study (diversifying/relaxing selection) might represent
571 this new shift. Interestingly, *T. immigrans*, which inhabit intermediate environmental
572 conditions (Figure 1c), shows also an intermediate pattern of *k*, with an intriguing

bimodal distribution (Figure 2b). Therefore, we can speculate that the highly skewed distributions point to ongoing adaptation to a colder climate, and a relaxation of selective forces present in warmer habitats. To our knowledge, this is the first time that this effect is found in an organism, most likely due to the underrepresentation of genomic studies on alpine and cold adapted species, and, importantly, the lack of application of the RELAXED test in a genome-wise manner.

Examining the effect of those evolutionary trajectories, metabolism seems to be significantly involved in the sub-alpine ant`s adaptation. Several clues are pointing in that direction, such as the presence of underground aphids in *T. alpestre* nests but not in those of *T. immigrans* (unpublished data), the expansion of OGs related to sugar transporters, and five enzymes under diversifying selection related to metabolism and phosphorylation of sugars. We deeply explored and validated one of these enzymes, Hex-T1, a key regulator and rate-limiting enzyme for energy (sugars) metabolism and reactive oxygen species (ROS) activity in insects (Xian-Wu and Wei-Hua 2016), by contrasting its enzymatic activity between *T. alpestre* and *T. immigrans*. We showed that the mutated form in *T. alpestre* is indeed overall more efficient, with less substrate needed to reach the highest reaction velocity of the enzyme, possibly due to a single amino acid mutation that enhance effect on the catalytic efficiency of the enzyme due to the formation of a more functional network of hydrogen bonds with its substrate. In fact, the path of the hydrogen bonds found in TalpHex-T1 resembled the one depicted by the X-ray solved structure of Hex-T1 from (Mulichak et al. 2002), used as a template to obtain the three-dimensional coordinates of both TimmHex-T1 and TalpHex-T1 (see Methods). Mulichak and colleagues identified their model residues Lys621 and Asp657 as crucial for the

597 catalytic activity of the protein; the corresponding residues TalpHex-T1$_{K168}$ and
598 TalpHex-T1$_{D204}$ are indeed interacting, together with other residues, with glucose in
599 TalpHex-T1 at both 6 and 26 °C. On the other hand, while the interaction with
600 TalpHex-T1$_{D204}$ is conserved, the one with the lysine is lost in TimmHex-T1 and a
601 looser protein-sugar network is formed, explaining the higher catalytic efficiency of
602 TalpHex-T1 versus that of TimmHex-T1. We can indeed infer that the higher
603 flexibility conferred by TalpHex-T1$_{G74}$ increases the shift of the residue TalpHex-
604 T1$_{K168}$, belonging to the catalytic site (Figure 4d, e), allowing it to move closer and
605 establish a stronger interaction with glucose, possibly contributing to lower the Km
606 of the catalytic reaction. In eco-evolutionary terms all these findings hint at a more
607 intimate relation between *T. alpestre* and the aphids. This relationship of ants and
608 aphids is one of the most studied mutualistic relationships in the animal kingdom.
609 Aphids produce honeydew, and in return ants offer protection from predators,
610 parasitoids, fungal infection and adverse conditions. Honeydew contains
611 monosaccharides (glucose and fructose), disaccharides (maltose, sucrose), and
612 Melezitose, a trisaccharide, that is one of the main sugar synthesized by aphids, and
613 which has been found to attract ants and maintain the ant-aphid mutualism (Fischer
614 and Shingleton 2001). Small amounts of amino-acids, proteins, and lipids are also
615 present (Pringle et al. 2014). Usually, this interaction is above ground level, on plant
616 leaves and branches, but there are cases in which ants are specialized to farm
617 subterranean aphids, just like in *Lasius flavus* (Ivens et al. 2012). *Tetramorium*
618 *alpestre* may have evolved the same behavior through a coevolution of physiological
619 factors such as palatability, fluid intake rate and digestibility of sugar molecules,

620 improving the ants' survival by enhancing energy intake, a limiting factor in high-
621 elevation ecosystems.

622 The complete annotation and characterization of the five HSP subfamilies in
623 19 ant species show good overall conservation, and strong purifying selection was
624 observed in most subfamilies. The exception are sHsps, which seem to be the most
625 diversified HSP subfamily, with the highest and the widest range of ω. It is also the
626 only subfamily that took a different evolutionary path compared with Diptera,
627 having very few orthologs in common with them. Given that sHsps are virtually
628 ubiquitous molecular chaperones that can prevent the irreversible aggregation of
629 denaturing proteins (Haslbeck and Vierling 2015), they may have played a central
630 role in the adaptation of ants to strongly different climates and environments.
631 Although we observe a higher distribution of ω in *T. alpestre*, no HSPs show a
632 significant sign of diversifying selection. Rather, six loci show relaxed purifying
633 selection (Hsp90: *Trap1*; Hsp60:*CCT4*, *CCT5*; Hsp40: *Sec63*, *DnajC8*, *DnajC11*). The
634 impact of the TNF receptor-associated protein (Trap1) on cellular bioenergetics of *T.*
635 *alpestre* may contribute to its adaptation to cold environments by differently
636 modulating cellular metabolism. Given that it functions as a negative regulator of
637 mitochondrial respiration, able to modulate the balance between oxidative
638 phosphorylation and aerobic glycolysis, possibly another form of metabolic
639 adaptation. It has been shown that reduced or absent *Trap1* expression leads to
640 deregulated mitochondrial respiration, that is, a high energy state characterized by
641 elevated ATP and reactive oxygen species, an increase in mitochondrial respiration
642 and fatty acid oxidation, and a cellular accumulation of tricarboxylic acid cycle
643 intermediates (Yoshida et al. 2013). *Trap1* overexpression is associated with

644 increased expression of genes associated with cell proliferation (Liu et al. 2010a).
645 Since the two Hsp60s are associated to protein folding and cytoplasmic microtubule
646 organization, biological processes also enriched by genes under diversifying
647 selection, this suggests profound changes in the cellular physiology of *T. alpestre*. It
648 is also plausible that adapting to a cold environment will depress selection on genes
649 directly related to severe heat shock. As we have shown, *T. alpestre*'s habitat is
650 characterised by temperatures that rarely exceed 20 °C (median = 16.5 °C; 99%
651 confidence interval = 17.8 °C), although rocky habitats may produce warmer
652 microhabitats. This could mean that this species experienced relaxed selection for
653 HSPs associated with the denaturation to protein folding by heat shock, as suggested
654 by the relaxation of purifying selection on *Cct5* and the three Hsp40s associated with
655 responses to heat and temperature stimulus.

656 Although we provide a range of evidence that adaptation to cold
657 environments can be related to changes in protein-coding sequences, it has long
658 been postulated that phenotypic divergence between closely related species, such as
659 *T. alpestre* and *T. immigrans*, is primarily driven by quantitative and spatiotemporal
660 changes in gene expression, mediated by alterations in regulatory elements (e.g.:
661 Danko et al., 2018; Prescott et al., 2015). We tested this hypothesis by looking at the
662 expression patterns of *stv* and four other HSPs (*Hsc70-4d*, *Hsc70-4e*, *Hsp83*, *l(2)efl4*),
663 between *T. alpestre* and *T. immigrans*. *Stv* is a member of Bcl-2-associated
664 athanogene (BAG)-family proteins, which interact with Hsc70s and Hsp70s, and can
665 modulate, either positively or negatively, the functions of these chaperones (Doong
666 et al. 2002). It is implicated in the recovery from chill shock in *D. melanogaster*
667 during cold recovery (Colinet and Hoffmann 2010, 2012). The concerted synthesis of

668 *D. melanogaster stv* and Hsp70s suggests cooperation to offset cold injury, possibly
669 by preserving the folding/degradation and by regulating apoptosis (Colinet and
670 Hoffmann 2010). In our experiment, an acute cold stress (-6 °C) was used to knock
671 down individuals. By looking at the differential expression of these genes in coma
672 and non-coma individuals within and between species, we were not only able to
673 show that *stv* may interact with Hsc70s, but also that *T. alpestre* has a quicker
674 response in these genes compared with, *T. immigrans,* the related species not cold
675 adapted. Given these results, which are in line with the selection signature we
676 identified, it is probable that *stv* may play a similar role in the physiology of ants. As
677 we have shown in this study, ants completely lack Hsp70s (Figure S14) and retained
678 only the heat shock cognates (Hsc70s) with mainly two conserved paralogs (*Hsc70-*
679 *4d* and *Hsc70-4e*), which may have evolved to function as the Dipteran Hsp70s.
680 Although we found an interesting and promising correlation between chill shock, *stv*,
681 and Hsc70s, it will be important to continue exploring other expression patterns in
682 ant physiology to assess whether *stv* has tissue-specific expression patterns, as was
683 found in *D. melanogaster* (Coulson et al. 2005), and to study its expression across
684 different species with different ecological adaptations.

685 One of the most enduring problems of evolutionary biology is explaining how
686 complex adaptive traits originate (Wagner and Lynch 2010). Although it is widely
687 assumed that new traits arise solely from selection on genetic variation, many
688 researchers ask whether phenotypic plasticity precedes and facilitates adaptation
689 (Levis and Pfennig 2016). This alternative scenario, the plasticity-first hypothesis,
690 states that under novel conditions, environmentally induced variation can be refined
691 by selection and, depending on whether plasticity is favoured, become

692 developmentally canalized through genetic assimilation. Under this scenario,
693 environmentally induced phenotypic change can precede and promote the
694 evolutionary origins of a complex adaptive trait.

695 Four criteria have been proposed for verifying this hypothesis (Levis and
696 Pfennig 2016): 1) the focal trait needs to be environmentally induced in the
697 ancestral-proxy lineages; 2) cryptic genetic variation will be uncovered when
698 ancestral-proxy lineages experience the derived environment; 3) the focal trait will
699 exhibit evidence of having undergone an evolutionary change in its regulation, in its
700 form, or in both in the derived lineages; and 4) the focal trait will exhibit evidence of
701 having undergone adaptive refinement in the derived lineages. Although it is
702 methodically difficult to prove each point, our findings on the evolution and
703 adaptation of *T. alpestre* appear consistent with plasticity-first evolution. In more
704 detail, *T. immigrans*, the ancestral-proxy lineage, shows considerable plasticity under
705 variable temperature conditions compared to other ant species (Criterion 1, Figure
706 1c), showing an ability to recover from severe chill-shocks that is almost as good as
707 the derived lineage (*T. alpestre*), and, unexpectedly, better efficiency of Hex-t1 at
708 lower rather than higher temperatures (Figure 4a). We suggest that the derived
709 lineage, *T. alpestre*, underwent genetic assimilation of the cold response (Criterion
710 3), followed by evolutionary refinement via changes in regulation, resulting, for
711 example, in *stv* differential expression (Criterion 4). Consistent with evolutionary
712 refinement, the derived lineage has evolved more extreme traits such as an overall
713 improved activity of Hex-T1 with reduced variability.

714 Our comparative genomic analysis shows how natural selection could trigger
715 complicated patterns of change in genomes, especially protein-coding sequences,

716 both in terms of diversifying selection and relaxation of purifying selection. Many of
717 these changes are in genes that may be associated with aspects of development,
718 either directly or through the associated complex changes in ecology and natural
719 history, and all of these hypotheses are now open for in-depth scrutiny.
720 Furthermore, this work identifies promising gene expression patterns that are
721 possibly playing an important role in adaptation to new ecological niches. Overall,
722 this study represents the first systematic attempt to provide a framework for the
723 genomic analysis of adaptation to extreme environments and underlines the
724 importance of studying organisms with different ecological niches in understanding
725 the genetic basis of ecological adaptation.
726
727
728 ## *Methods*
729 ### Species-locality and climatic data
730 To define the environment of *T. alpestre* and the other four *Tetramorium* species,
731 georeferenced occurrence data were compiled and complemented with those for
732 the native ranges of other ant species with available genomic data. Occurrence
733 records for 17 species (Table S2) were compiled from the Global Ant Biodiversity
734 Informatics database (GABI, Guénard et al., 2017, accessible via www.antmaps.org,
735 Janicki et al., 2016). The species determinations in the records were evaluated by
736 specialists in ant taxonomy, and erroneous data were excluded. Slightly incorrect
737 coordinates (i.e. in the ocean within 8.5 km of land) were assigned to the nearest
738 land point. Additionally, georeferenced occurrence data of two species (*T. alpestre,*
739 *T. immigrans*) were compiled from the latest taxonomic revision (Wagner et al.

2017). The occurrence data of each species were spatially rarefied at a 5 km level using the R package SPTHIN v. 0.1.0 (Aiello-Lammens et al. 2015), to counter spatial autocorrelation and to provide some protection against sampling bias issues (Merow et al. 2013). The Bioclim variables bio1-bio19 from the WORLDCLIM database v. 1.4 (Hijmans et al. 2005) were extracted for each unique species locality at a 2.5 arc min resolution (4.65 x 4.65 = 21.6225 km^2 at the equator) using ARCGIS v. 10.4 (ESRI, Redland, CA). A Wilcoxon-Mann-Whitney rank sum test as implemented in the R package WILCOX.TEST (http://www.r-project.org) was adopted to test for differences between *T. alpestre* and the other species individually for each of the Bioclim variables. The Bonferroni-Holm sequential rejection procedure (Abdi 2010) was used to control for multiple testing.

Biological sample processing, genome size estimation, and genome sequencing

Six colonies of *T. alpestre* ants were sampled, two for flow cytometry (nest 18811: Penser Joch, Italy, 46.83379° N, 11.44652° E, 21 June 2016; nest 18813: Kühtai, Austria, 47.27923, 11.07590° E, 21 June 2016), three for RNA extraction (nest 18586: Zirmbachalm, Austria, 47.21920° N, 11.07530° E, 30 July 2015; nest 18590: Zirmbachalm, 47.21910° N, 11.07620° E, 30 July 2015; nest 18594: Penser Joch, 46.82940°N, 11.43830° E, 2 August 2015), and one for DNA extraction (nest 18592: Penser Joch, 46.83380° N, 11.44610° E, 2 August 2015). The ants were brought alive to the laboratory (for flow cytometry) or immediately submerged in RNAlater (for RNA extraction) or 96% ethanol (for DNA extraction) and stored at -70 °C (RNA) or -20 °C (DNA).

763 Flow cytometry was used to estimate relative genome size from single *T.*
764 *alpestre* worker heads, using strain ISO-1 of *Drosophila melanogaster* as internal
765 standard (obtained from Bloomington Drosophila Stock Center, Indiana University,
766 Bloomington, USA; nuclear DNA content: 0.35 pg, Gregory 2018). Six individuals each
767 were measured from *T. alpestre* nests 18811 and 18813. In more detail, single *T.*
768 *alpestre* heads and, separately, heads of 10 ISO-1 females were chopped in 500 µL of
769 ice-cold Otto 1 Buffer (0.1 mol/L citric acid, 0.5% Tween20 (Merck KGaA, Darmstadt,
770 Germany)). The suspensions were filtered using 42-µm nylon meshes and incubated
771 for 5 min. Then, 1 mL of staining solution (DAPI (4 µL/mL) and 2-mercaptoethanol (2
772 µL/mL) in Otto 2 buffer (0.4 mol/L $Na_2HPO_4 \cdot 12$ H2O)) was added to each suspension.
773 For each measurement, 200 µL suspension of a single *T. alpestre* worker and 10 µL of
774 the ISO-1 standard were used. Fluorescence intensity of 3000 cell nuclei per sample
775 was measured with a Partec CyFlow space flow cytometer (Partec GmbH, Münster,
776 Germany). Gating and peak analysis were done automatically using the software
777 Partec Flo Max.

778 For the DNA and RNA extractions, the individuals were thawed on ice and the
779 gasters removed. DNA was extracted using the QIAamp DNA Micro Kit (Qiagen). The
780 extraction followed the protocol of the manufacturer, except that 20 µl RNase A
781 solution (Sigma-Aldrich) was added to the vials and incubated for 5 minutes at room
782 temperature. DNA concentration and quality were checked via Nanodrop (Thermo
783 Scientific) and gel electrophoresis. Two adult males were used to generate the
784 overlapping-read and the paired-end (PE) libraries, while for the mate-pair (MP)
785 libraries, four adult females were extracted of nest 18592. RNA was extracted using
786 the RNeasy Mini Kit (Qiagen) following the instructions of the manufacturer. Six

787 developmental stages were extracted as pools of individuals (nest 18586: worker
788 larvae – 30 individuals, worker pupae – 40, worker adult – 50; nest 18594: gyne
789 pupae – 2; nest 18590: gyne adult – 7, male adult – 7). RNA concentration and
790 quality were checked via Nanodrop (Thermo Scientific) and gel electrophoresis.

791 All *T. alpestre* DNA-seq and RNA-seq Illumina libraries were prepared by
792 IGATech (http://igatechnology.com/). Specifically, four libraries were used for
793 genome sequencing of *T. alpestre*: one overlapping-reads library (insert size ~400 bp;
794 paired-end (PE) sequencing with 2×250 bp read length), one regular PE library (insert
795 size ~400 bp, 2×100 bp read length), and two mate pair libraries (insert size ~4 kb,
796 2×100 bp read length) (see Table S2). For RNA-seq, six strand-specific libraries (insert
797 size ~500 bp, 2×200 bp read length) were constructed from three stages of workers
798 (larvae, pupae, adult), two stages of gynes (larvae and adult), and adult males. All
799 libraries were sequenced on an Illumina HiSeq 2500 platform in standard (DNA) and
800 RAPID (RNA) mode. For each *T. immigrans*, *T. bicarinatum*, *T. simillimum*, and *T.*
801 *parvispinum*, one TrueSeq library (insert size ~500 bp, 2×100 bp read length) was
802 prepared and sequenced on an Illumina HiSeq 4000 machine at OIST sequencing
803 center.

804

805 **Genomic and mitogenomic assembly and gene prediction**

806 Genomic sequencing reads of *T. alpestre* were filtered to remove low-quality reads
807 and PCR duplicates, corrected, and assembled using ALLPATHS-LG v. 52488 (Gnerre et
808 al. 2011). Contigs were first constructed based on overlapping reads and then
809 scaffolded using paired-end and mate-pair information from all DNA libraries. Given
810 the high coverage of the overlapping reads, based on the estimated genome size,

811 multiple trials were performed using different coverages to establish the best
812 combination of read coverage. The genomes of the other four related species were
813 assembled using SPADES v. 3.10.0 (Bankevich et al. 2012) with enabled read error
814 correction algorithm, a *k*mer range of 21, 33, 55, 77, 99, and mismatch correction.
815 Scaffolds belonging to contaminants were identified and removed using BLOBOLOGY v.
816 2013-09-12 (Kumar et al. 2013).

817 A bioinformatic pipeline that included combinatorial approaches of
818 homology, *ab initio*, and *de novo* methods were implemented to predict gene
819 models. REPEATMASKER v. 4.0.6 (Smit et al. 2013) was used to generate repeat hints.
820 For the homology-based exon hints, protein data sets of *D. melanogaster*, *Apis*
821 *mellifera*, *Nasonia vitripennis*, and 12 ant species (see Table S1) were aligned to the
822 *T. alpestre* genome using TBLASTN (*e*-value cut-off: $1e^{-5}$) and EXONERATE v. 2.2.0
823 (Slater and Birney 2005). As an *ab initio* procedure, the merged RNA-seq libraries
824 were mapped using STAR v. 020201 (Dobin et al. 2013) (settings: ALIGNENDSTYPE Local;
825 ALIGNINTRONMIN 30; ALIGNINTRONMAX 450,000; OUTSJFILTERINTRONMAXVSREADN 80 100
826 500 1000 2000 5000 20,000; ALIGNSJOVERHANGMIN 10; ALIGNTRANSCRIPTSPERREADNMAX
827 100,000) to generate the splice-site position-specific scoring matrix (PSSM) and
828 CUFFLINKS v. v2.2.1 (Trapnell et al. 2012) to generate UTR and intron hints. This
829 information was then integrated with GENEMARK-ES v. 4 (Hoff et al. 2015) to train the
830 analysis and use the outcome under the BRAKER1 procedure (Hoff et al. 2015) and
831 AUGUSTUS v. 3.2.1. (Stanke et al. 2006). To avoid missing genes due to unassembled
832 regions of the genome, previously unmapped reads were *de novo* assembled using
833 TRINITY v. 2.2.0 (Grabherr et al. 2011) and annotated with FRAMA (Bens et al. 2016).
834 The three results where then merged, and Benchmarking Universal Single Copy

Orthologs (BUSCO v. 1.2) (Simão et al. 2015) was adopted to evaluate the annotation completeness together with integrity and completeness evaluation using DELTABLAST (Boratyn et al. 2012). A visual inspection of the annotation and gene integrity was also performed on more than 250 loci.

All available complete ant mitochondrial genomes (mtDNA) were downloaded from GENBANK (Benson et al. 2014) (Table S1). Illumina raw SRA data of other ant species were downloaded and processed following Cicconardi et al., (2017b). In brief, reads were quality filtered and assembled using IDBA-UD v. 1.1.1 (Peng et al. 2012) and SPADES v. 3.10.0 (Bankevich et al. 2012), and annotated using MITOS v. 2 web server (Bernt et al. 2013).

Phylogenetic analysis

Nuclear single-copy ortholog genes (scOGs) and complete mitochondrial genomes were used to compute the ant species tree. Once scOGs were determined (see below), single-locus trees and a species tree of concatenated scOGs were estimated using Maximum Likelihood (ML) search as implemented in FASTTREE v. 2.1.8 SSE3 (Price et al. 2010). Gene trees were summarized with MP-EST (Liu et al. 2010b) using the STRAW web-server (Shaw et al. 2013).

For the mtDNA phylogeny, only protein-coding genes were used. Each gene was aligned using MACSE v. 1.01b (Ranwez et al. 2011), and all alignments were concatenated. The best partitions and models of evolution were identified with PARTITIONFINDER v. 1.1.1_Mac (Lanfear et al. 2014). MtDNA trees were searched with ML and Bayesian Inference (BI) algorithms. For ML, GARLI v. 2.01.1067 (http://code.google.com/p/garli) was used performing 20 + 5 runs from random

859 starting trees. The runs were continued until no further improvement in log-
860 likelihood was found, followed by 1000 bootstrap pseudoreplicates. The results were
861 summarized using SUMTREES v. 3.3.1 (http://bit.ly/DendroPy), using *A. mellifera*, *N.*
862 *vitripennis*, and *D. melanogaster* as outgroups. For BI, BEAST v. 2 (Bouckaert et al.
863 2014) was adopted to obtain the dated mtDNA tree and to estimate the divergence
864 of the most recent common ancestors (MRCAs) (template: BEAST (Heled and
865 Drummond 2010)). Fossil data were taken mainly from Moreau & Bell (2013) and
866 PALEOBIO DB (paleobiodb.org) (see Table S4 for a detailed list of references) and used
867 as minimum calibration points constraining nodes in the topology as listed in Table
868 S4. Lognormal prior distribution was implemented with an offset corresponding to
869 the minimum fossil age, log(mean) of 1.0, and log(SD) of 1.0. Ten independent runs
870 of 8 x 10^7 generations were sampled every 100,000th generation. Each partition was
871 modelled with an uncorrelated relaxed clock with a Yule process, species tree prior,
872 and its best substitution model. Evolutionary models not implemented in BEAUTI v2
873 (Bouckaert et al. 2014) were manually edited in the xml file. TRACER v. 1.6
874 (http://beast.bio.ed.ac.uk/Tracer) was used to evaluate convergence and the
875 parameters' effective sampling size (ESS) and a burn-in was manually implemented
876 and roughly 10% from each run were removed. LOGCOMBINER (Bouckaert et al. 2014)
877 and TREEANNOTATOR (Bouckaert et al. 2014) were used to summarize the results in a
878 single consensus tree. The non-ant species were excluded from the analysis, and no
879 outgroup was adopted. Divergence dates for the maximum-likelihood nuclear DNA
880 (nuDNA) tree (only ants) were also inferred using the penalized likelihood approach
881 (Sanderson 2002) implemented in the R package APE v. 5.1 (Paradis et al. 2004) by

882 calibrating four nodes: the root, the *Tetramorium*, the *Solenopsis*+*Monomorium*, and
883 the Attini branches (Table S4).
884
885 **Functional annotation and orthologous-group dynamic evolution**
886 Genes from 19 ant and three outgroup species (Table S3) were clustered into
887 ortholog groups (OGs) with HIERANOID v. 2 (Kaduk and Sonnhammer 2017), which
888 implements INPARANOID v. 8 (Sonnhammer and Östlund 2015) using a guide tree
889 topology based on Moreau & Bell (2013) and BLASTP (*e*-value cutoff of 10^{-5}) to
890 improve the reciprocal hit accuracy (Edgar 2010), while homology relationships were
891 searched with DELTABLAST (Boratyn et al. 2012). The functional annotation of each
892 putative protein coding sequence was performed by identifying both the protein
893 domain architecture and Gene Ontology (GO) terms. For each sequence, first
894 HMMER v. 3.1b2 (HMMSCAN) (Eddy 2011) was used to predict PFAM-A v. 31.0 domains,
895 then Domain Annotation by a Multi-objective Approach (DAMA) v. 2 (Bernardes et
896 al. 2015) was applied to identify architectures combining scores of domain matches,
897 previously observed multi-domain co-occurrence, and domain overlapping.
898 Annotation of GO terms was performed as implemented in the CATH assignments
899 for large sequence datasets (Das et al. 2015). Briefly, each input sequence was
900 scanned against the library of CATH functional families (FUNFAMS) HMMs (Sillitoe et
901 al. 2015) using HMMER3 (Eddy 2011) to assign FUNFAMS to regions on the query
902 sequence (with conditional *E*-value < 0.005). Then the GO annotations for a
903 matching FUNFAM were transferred to the query sequence with its confidence scores,
904 calculated by considering the GO term frequency among the annotated sequences.

905 Finally, a non-redundant set of GO annotations was retained, making up the GO
906 annotations for the query protein sequence (Sillitoe et al. 2015).

907 To identify orthologous groups specifically expanded in the *T. alpestre*
908 genome, BADIRATE v. 1.35 (Librado et al. 2012) was performed twice, once for the
909 nuDNA and one for the mtDNA ultrametric tree topologies, reconstructing ancestral
910 family sizes, gain, death, and innovation (GDI), applying stochastic models and
911 allowing estimation of the family turnover rate (λ) by ML. Using this approach, we
912 observed a correlation between the turnover rate (λ) and branch lengths (Spearman
913 correlation: ρ = -0.52, *P*-value = 0), and a bimodal distribution of λ. We interpreted
914 the distribution closer to 0 as background noise and therefore considered only
915 expanded and contracted OGs with λ within the second distribution. The boundary
916 between the two distributions was defined by the valley values between the two,
917 which were computed using OPTIMIZE and APPROXFUN functions implemented in the
918 STATS v. 3.4.0 package in R.

919

920 **Heat-shock protein family analysis**

921 From the functional annotation analyses of all Hymenoptera, all sequences bearing a
922 valid protein domain matching HSPs were extracted and aligned using the CLUSTALW
923 v.1.2.1 EBI web server (Larkin et al. 2007) (settings: MBED true; MBEDITERATION true;
924 ITERATIONS 5; GTITERATIONS 5; HMMITERATIONS 5). A phylogenetic tree was computed
925 using ML as implemented in FASTTREE v. 2.1.8 SSE3 (Price et al. 2010) and manually
926 checked to identify and provisionally annotate the five main subfamily proteins
927 (Hsp90, Hsp70, Hsp60, Hsp40, and sHsp) and their OG. Sequences falling outside
928 clusters and with low bootstrap values were manually checked with the DELTABLAST

(Boratyn et al. 2012) web-server and with the CONSERVED DOMAIN DATABASE (CDD) web-server (Marchler-Bauer et al. 2017) to identify and remove bacterial contaminants and spurious/incomplete sequences. Then, nucleotide sequences belonging to each subfamily were revers translated into amino acids, aligned using CLUSTALW v.1.2.1, and the obtained protein alignment was used to derive the nucleotide one. FASTTREE was used again to compute phylogenetic trees for the five HSP subfamilies.

Selection on single-copy orthologous groups and gene families

All selected scOGs and HSP-OGs were scanned to evaluate selection signature on coding regions of *T. alpestre*. This was done by computing the mean ω and the relaxation of each branch of the phylogeny of *Tetramorium* spp. + *Vollenhovia emeryi*. More specifically, adopting a pipeline similar to that in Cicconardi et al. (2017a, 2017b), the signatures of diversifying selection were searched in codon-based aligning groups of one-to-one orthologous ant genes with MACSE v. 1.01b (Ranwez et al. 2011), filtering with GBLOCKS v. 0.91b (Castresana 2000) under a "relaxed" condition (Parker et al. 2013; Cicconardi et al. 2017a, 2017b) and using the aBSREL algorithm as implemented in the HYPHY batch language (Kosakovsky Pond et al. 2005) using a batch script (BRANCHSITEREL) in HYPHY (http://github.com/veg/hyphy).

In parallel, the same scOGs and HSP-OGs were scanned using the RELAX test (Wertheim et al. 2014) to search for putative signals of relaxation. In brief, RELAX tests the hypothesis of evolutionary-rate relaxation in selected branches of a phylogenetic tree compared with reference branches. A *k* value is computed to evaluate whether the selective strength ω shifts towards neutrality. The rate of d_N/d_S

(ω) can relax (k < 1), stay stable (k = 1), or intensify (k > 1). For both scOGs and HSP-OGs, and for both the ABSREL and RELAX tests, the Bonferroni-Holm sequential rejection procedure (Abdi 2010) was used to control the false discovery rate with a very stringent cutoff value of 0.005 for the adjusted *P*-values applied (Benjamin et al. 2017). Hsp60s and Hsp40s under relaxed selection were analyzed using the GENEMANIA prediction server (Warde-Farley et al. 2010) to predict their functions by creating an interaction network with genes by including protein and genetic interactions, pathways, co-expression, co-localization, and protein domain similarity.

Finally, the GOSTATS package for R (Falcon and Gentleman 2007) (settings: ANNOTATION org.Dm.eg.db; CONDITIONAL TRUE; TESTDIRECTION over) was used to check for GO terms of biological processes and KEGG pathway enrichments of scOGs under selection and relaxation using the whole set of tested scOGs as background. *P*-values < 0.005 and < 0.05 were implemented for GO terms and KEGG pathways, respectively.

Synthesis of Hex-t1 gene and its enzyme activity assays

Following identification as under diversifying selection in *T. alpestre* (see results section "Dual signature of evolutionary pressures in single-copy OGs in the *T. alpestre* genome"), synthesis of genes and enzymes was attempted for phosphofructokinase, transketolase, phosphoglucosemutase, and Hex-t1 was successful just for the Hex-t1. In more detail, the Hex-t1 genes of *Tetramorium alpestre* (1398 bp) and *T. immigrans* (1386 bp) were synthesized by ThermoFisher lifetechnologies (Carlsbad, CA, USA) and Eurofins Genomics (Ebersberg, Germany), respectively. Both constructs carried a 5' EcoRI and a 3' HindIII recognition site for

977 subsequent cloning as well as a C-terminal His-tag. The genes were excised from
978 their carrier backbones by enzymatic digestion. The fragments were purified by
979 agarose gel excision and sub-cloned into the pACEBac1 expression vector
980 (MULTIBACTM, Geneva Biotech, Geneva, Switzerland). Correct insertion was verified
981 by Sanger sequencing, and transformation into *Drosophila melanogaster* cells and
982 protein expression followed the standard protocols of the expression vector
983 manufacturer. After cell harvesting, the presence of the recombinant protein in the
984 cell lysates was verified by a western blot targeting the His-tag. The relative amounts
985 of protein were quantified from the western blot using ImageJ
986 (https://imagej.net/Welcome). The cell lysates were centrifuged at 4000 rpm at 4 °C
987 for 5 min, and the supernatant was directly used as protein source.

988 Enzyme activity assays followed a modified protocol of Crabtree &
989 Newsholme (1972). Briefly, 1000 µl assay medium containing 75 mM Tris pH=7.5
990 (Merck Millipore, Burlington, MA, USA), 7.5 mM $MgCl_2$ (Merck), 0.8 mM EDTA
991 (Sigma-Aldrich, St. Louis, MO, USA), 1.5 mM KCl (Merck), 4.0 mM mercaptoethanol
992 (Sigma), 0.4 mM NADP+ (Abcam, Cambridge, UK), 2.5 mM ATP (Abcam), and 10 mM
993 creatine phosphate (Abcam) were placed in a disposable cuvette (Brand, Germany)
994 in a SPECORD 210 PLUS UV/VIS spectrophotometer (Analytic Jena AG, Germany)
995 with an attached 1157P programmable thermostate (VWR, Radnor, PA, USA).
996 Variable amounts of D-glucose (VWR) and synthetic protein were added, and the
997 cuvette was allowed to reach the assay temperature. Then, the reaction was started
998 by adding 15 U creatine phosphokinase (Sigma) and 5 U glucose 6-phospahte
999 dehydrogenase (Sigma).

The Hex-t1 activity was measured in triplicate as the rate of reduction of $NADP^+$ causing an extinction at 340 nm. Each measurement lasted for 60 s, and every second, an extinction value was recorded. For the determination of the Michaelis-Menten constant (Km-value) of both enzymes, assays were conducted along a substrate gradient from 0.00167 to 24.30000 mM D-glucose, achieving saturated extinction curves. Assay temperatures ranged from 6 °C to 36 °C with 10 K increments. The software PRISM v. 8 (GraphPad Software, San Diego, CA, USA) was used to calculate the Km-values.

Hex-t1 structure modelling and molecular dynamics simulations

The three-dimensional structures of *T. alpestre* and *T. immigrans* Hex-t1 proteins are not available. To study the effect of the amino acid changes on the proteins' function/dynamics, we modeled the structures of these two proteins via homology modelling. The X-ray structure of the Hex-t1 isoform from *Schistosoma mansoni* (Mulichak et al. 2002), solved at 2.6 Å resolution was used as a template and the models were generated using the software MODELLER v. 9.21 (Webb and Sali 2014). Once we obtained the models, we built the simulative systems to run molecular dynamics simulations. The two proteins TalpHex-t1 and TimmHex-t1, in complex with the glucose substrate, were immersed in a triclinic box filled with TIP3P water molecules (Jorgensen et al. 1983) and rendered electroneutral by the addition of cloride counterions. The topology of the two systems, consisting of ~ 80.000 atoms each, was built using the AMBER14 force field (Case et al. 2014), further converted in GROMACS v. 4.6 (Hess et al. 2008) format using ACPYPE (Sousa Da Silva and Vranken 2012). Simulations were run on a GPU cluster using GROMACS v. 4.6 with the following

protocol: 1) 25000 steps of steepest descent followed by 25000 steps of coniugate gradient minimization; 2) 5*100 ps of equilibration runs in the NVT environment starting at 50 K and performed by increasing the temperature of 50 K after each run untill a final value of 250 K; 3) 5*100 ps of equilibration runs in the NPT environment starting at 50 K and performed by increasing the temperature of 50 K after each run untill a final value of 250 K; 4) the equilibrated systems were simulated for 500 ns at 279 or 300 K, i.e. at 6 or 26 °C, for a total of four simulations and 2 µs of sampling. Electrostatic interactions were considered by means of the Particle Mesh Ewald method (PME) with a cut off of 1.2 nm for the real space and Van der Waals interactions (Darden et al. 1993). Bond lengths and angles were constrained via the LINCS algorithm (Hess et al. 1997). The temperatures were kept constant at 279 or 300 °K by using the velocity rescale with a coupling constant of 0.1 ps, and the pressure was kept at 1 bar using the Parrinello-Rahman barostat with a coupling constant of 1.0 ps during sampling (Parrinello and Rahman 1981). The four trajectories were collected and comparative analyses performed with the GROMACS suite or with in house written code.

Chill coma assay and quantitative qRT-PCR assay

The cold hardiness and expression of selected genes were compared between *T. alpestre* and *T. immigrans* using chill coma assays. From four colonies additional to those used for other experiments in this study, two per species, about 500 workers per colony were collected in August 2017; *T. alpestre*: Jaufenpass (18980: 46.83791° N, 11.29768° E) and Penser Joch (18978: 46.81402° N, 11.44198° E); *T. immigrans*: Vienna (18977: 48.12448° N, 16.43522° E.; 18983: 48.31341° N, 16.42529° E).

Workers were collected alive using aspirators, transported to the laboratory in Innsbruck, and kept in polypropylene boxes (18.5 cm x 11 cm) with chambers of various sizes. The walls of the boxes were Fluon-coated (GP1, De Monchy International BV, Rotterdam, Netherlands) to prevent workers from escaping. Food (sugar-honey-water and deep-frozen *Drosophila* flies) and tap water were provided *ad libitum* three times a week. Workers were kept in a climate chamber (MIR-254, Panasonic, Etten Leur, Netherlands) at a 12L:12D photoperiod at constant 18 °C. The temperature of 18 °C was the average of the monthly mean temperatures experienced at 200 m a.s.l. (*T. immigrans*, approx. 23.7 °C) and at 2000 m a.s.l. (*T. alpestre*, approx. 12.3 °C) in July 2017. Workers were acclimatized to 18 °C for at least three weeks before the chill coma assays.

After the acclimation period, from each of the four colonies, 90 workers were randomly chosen and divided into 18 equivalent pools, each were used for the chill coma and for the control assays. For the chill coma assay, worker pools were transferred into empty 5-ml glass vials, sealed, and immersed for 6.5 hours in a water:ethane-1,2-diol mix (1:1) bath set at -6 °C; in pilot experiments, this temperature had been determined as the highest temperature at which the ants had fallen into chill coma after 6.5 hours exposition; the temperature was identical for both species. Temperature was monitored using an electronic thermometer (TFX 430, ebro Electronic GmbH; Ingolstadt, Germany) with an accuracy of 0.05 °C inserted into an additional, empty vial treated in the same way as the vials with ants. After chill coma, the vials were transferred to a climate chamber at 18 °C, and the workers were allowed to recover for 0.5, 2.0, and 4.0 hours. For each recovery time, three replicate pools were used. After recovery, the workers were transferred to

RNAse-free reaction tubes and killed in liquid nitrogen. Tubes were stored at -70 °C. For the control assay, worker pools were transferred to empty glass vials and placed in the climate chamber at 18 °C. After 6.5 hours plus respective recovery time, the workers were killed and stored as described above.

For each recovery time and replicate, complete worker pools were used for the molecular analyses. RNA was extracted using the NUCLEOSPIN® RNA Kit (Macherey-Nagel, Düren, Germany) following the instructions of the manufacturer. First-strand cDNA was synthesized using 200 U REVERTAID reverse transcriptase (all reagents by Thermo Fisher Scientific, Waltham, USA), 40 U RIBOLOCK RNASE inhibitor, 5 µM random hexamer primers, 100 µM dNTPs, and 2 µl RNA extract in a total volume of 40 µl. The mixture was incubated for 5 min at 25 °C, 60 min at 42 °C, and 5 min at 70 °C on a UnoCycler 1200 (VWR, Radnor, USA). Quantitative PCR was conducted on a Rotorgene Q (Qiagen) PCR system. Each reaction contained 1× Rotor-Gene SYBR Green PCR Mastermix (Qiagen), 0.2 µM of primers, specifically designed for target genes (Table S12), and 1 µl cDNA in a total volume of 10 µl. All qRT-PCR reactions were performed as triplicates. Cycling conditions were 95 °C for 5 min, followed by 40 cycles of 94 °C for 15 s, 58 °C for 10 s, and 72 °C for 15 s. Fluorescence was acquired at the end of each elongation step. PCR was followed by a melting curve analysis from 60 to 95 °C with 0.1 °C increments held for 5 s before fluorescence acquisition. Cycle threshold (Ct) values were subtracted from total number of cycles. On these values, linear-regression analyses were based separately for each target gene, treatment, recovery time, and species (in each regression analysis, two populations and three replicate values were used, i.e., n = 6) using the housekeeping gene as independent variable and the target gene as dependent

variable. For each target gene / recovery-time combination one-way analysis of covariance (ANCOVA) followed by Bonferroni-Holm correction was then used to identify significant differences between treatments within species and between species within treatment.

Data access

The sequence data from this study have been submitted to the National Center for Biotechnology Information (NCBI) Sequence Read Archive (SRA) under BioProject numbers PRJNA532334, PRJNA533534, PRJNA533535, PRJNA533536 and PRJNA533537 (https://www.ncbi.nlm.nih.gov/bioproject/). The mtDNA genome assemblies have been submitted to the NCBI (GenBank accessions: MK861047 - MK861070). All accession codes of deposited and retrieved data are provided in Table S1.

Acknowledgements

Philipp Andesner and Stefan Gross for valuable work in the laboratory. Research was supported by the Austrian Science Fund (FWF, P23409, P30861). The computational results presented here have been achieved in part by using the HPC infrastructure of the University of Innsbruck (LEO), the Vienna Scientific Cluster (VSC), the collaborative system of the Universities Innsbruck and Linz (MACH), and the Swiss National Supercomputing Centre (CSCS) hosted in Lugano.

References

Aiello-Lammens ME, Boria RA, Radosavljevic A, Vilela B, Anderson RP. 2015. spThin: An R package for spatial thinning of species occurrence records for use in ecological niche models. *Ecography (Cop)* **38**: 541–545.

Archambault V, Lépine G, Kachaner D. 2015. Understanding the Polo Kinase machine. *Oncogene* **34**: 4799–4807.

Bankevich A, Nurk S, Antipov D, Gurevich A a., Dvorkin M, Kulikov AS, Lesin VM, Nikolenko SI, Pham S, Prjibelski AD, et al. 2012. SPAdes: A New Genome Assembly Algorithm and Its Applications to Single-Cell Sequencing. *J Comput Biol* **19**: 455–477.

Benjamin DJ, Berger JO, Johannesson M, Nosek BA, Wagenmakers E-J, Berk R, Bollen KA, Brembs B, Brown L, Camerer C, et al. 2017. Redefine statistical significance. *Nat Hum Behav*. http://www.nature.com/articles/s41562-017-0189-z.

Bens M, Sahm A, Groth M, Jahn N, Morhart M, Holtze S, Hildebrandt TB, Platzer M, Szafranski K. 2016. FRAMA: from RNA-seq data to annotated mRNA assemblies. *BMC Genomics* 1–12. http://dx.doi.org/10.1186/s12864-015-2349-8.

Benson DA, Clark K, Karsch-Mizrachi I, Lipman DJ, Ostell J, Sayers EW. 2014. GenBank. *Nucleic Acids Res* **43**: D30–D35. http://nar.oxfordjournals.org/lookup/doi/10.1093/nar/gku1216.

Bernardes JS, Vieira FRJ, Zaverucha G, Carbone A. 2015. A multi-objective optimization approach accurately resolves protein domain architectures.

1143 *Bioinformatics* **32**: 345–353.

1144 Bernt M, Donath A, Jühling F, Externbrink F, Florentz C, Fritzsch G, Pütz J,

1145 Middendorf M, Stadler PF. 2013. MITOS: Improved de novo metazoan

1146 mitochondrial genome annotation. *Mol Phylogenet Evol* **69**: 313–319.

1147 http://dx.doi.org/10.1016/j.ympev.2012.08.023.

1148 Bertelsmeier C, Ollier S, Liebhold A, Keller L. 2017. Recent human history governs

1149 global ant invasion dynamics. *Nat Ecol Evol* **1**.

1150 https://www.nature.com/articles/s41559-017-0184.pdf.

1151 Bolton B. 2018. An online catalog of the ants of the world. Available from

1152 http://antcat.org.

1153 Boratyn GM, Schäffer AA, Agarwala R, Altschul SF, Lipman DJ, Madden TL. 2012.

1154 Domain enhanced lookup time accelerated BLAST. *Biol Direct* **7**: 12.

1155 http://www.ncbi.nlm.nih.gov/pubmed/22510480%5Cnhttp://www.pubmedcen

1156 tral.nih.gov/articlerender.fcgi?artid=PMC3438057.

1157 Bouckaert R, Heled J, Kühnert D, Vaughan T, Wu C-H, Xie D, Suchard M a, Rambaut A,

1158 Drummond AJ. 2014. BEAST 2: a software platform for Bayesian evolutionary

1159 analysis. *PLoS Comput Biol* **10**: e1003537.

1160 http://www.pubmedcentral.nih.gov/articlerender.fcgi?artid=3985171&tool=pm

1161 centrez&rendertype=abstract (Accessed May 27, 2014).

1162 Case DAA, Babin V, Berryman JTT, Betz RMM, Cai Q, Cerutti DSS, Cheatham TE, III,

1163 Darden TAA, Duke REE, et al. 2014. AMBER14. *Univ California, San Fr*.

1164 Christian KA, Morton SR. 1992. Extreme thermophilia in a central Australian ant,

1165 Melophorus bagoti. *Physiol Zool* **65**: 885–905.

1166 Cicconardi F, Di Marino D, Olimpieri PP, Arthofer W, Schlick-Steiner BC, Steiner FM.

2017a. Chemosensory adaptations of the mountain fly Drosophila nigrosparsa (Insecta: Diptera) through genomics' and structural biology's lenses. *Sci Rep* **7**: 43770. http://dx.doi.org/10.1038/srep43770.

Cicconardi F, Marcatili P, Arthofer W, Schlick-Steiner BC, Steiner FM. 2017b. Positive diversifying selection is a pervasive adaptive force throughout the Drosophila radiation. *Mol Phylogenet Evol* **112**: 230–243.

Clark MS, Worland MR. 2008. How insects survive the cold: molecular mechanisms—a review. *J Comp Physiol B* **178**: 917–933. http://link.springer.com/10.1007/s00360-008-0286-4.

Colinet H, Hoffmann A. 2010. Gene and protein expression of *Drosophila* Starvin during cold stress and recovery from chill coma. *Insect Biochem Mol Biol* **40**: 425–428. http://dx.doi.org/10.1016/j.ibmb.2010.03.002.

Colinet H, Hoffmann AA. 2012. Comparing phenotypic effects and molecular correlates of developmental, gradual and rapid cold acclimation responses in Drosophila melanogaster. *Funct Ecol* **26**: 84–93.

Coulson M, Robert S, Saint R. 2005. Drosophila starvin encodes a tissue-specific BAG-domain protein required for larval food uptake. *Genetics* **171**: 1799–1812.

Danko CG, Choate LA, Marks BA, Rice EJ, Wang Z, Chu T, Martins AL, Dukler N, Coonrod SA, Tait Wojno ED, et al. 2018. Dynamic evolution of regulatory element ensembles in primate CD4+ T cells. *Nat Ecol Evol* **2**. http://www.nature.com/articles/s41559-017-0447-5.

Darden T, York D, Pedersen L. 1993. Particle mesh Ewald: An N·log(N) method for Ewald sums in large systems. *J Chem Phys*.

Das S, Sillitoe I, Lee D, Lees JG, Dawson NL, Ward J, Orengo CA. 2015. CATH

1191 FunFHMMer web server: Protein functional annotations using functional family
1192 assignments. *Nucleic Acids Res* **43**: W148–W153.
1193 Dobin A, Davis C a, Schlesinger F, Drenkow J, Zaleski C, Jha S, Batut P, Chaisson M,
1194 Gingeras TR. 2013. STAR: ultrafast universal RNA-seq aligner. *Bioinformatics* **29**:
1195 15–21.
1196 http://www.pubmedcentral.nih.gov/articlerender.fcgi?artid=3530905&tool=pm
1197 centrez&rendertype=abstract.
1198 Doong H, Vrailas A, Kohn EC. 2002. What's in the "BAG"? - A functional domain
1199 analysis of the BAG-family proteins. *Cancer Lett* **188**: 25–32.
1200 Eddy SR. 2011. Accelerated profile HMM searches. *PLoS Comput Biol* **7**.
1201 Edgar RC. 2010. Search and clustering orders of magnitude faster than BLAST.
1202 *Bioinformatics* **26**: 2460–2461.
1203 Falcon S, Gentleman R. 2007. Using GOstats to test gene lists for GO term
1204 association. *Bioinformatics* **23**: 257–258.
1205 Fischer MK, Shingleton AW. 2001. Host plant and ants influence the honeydew
1206 sugar. *Funct Ecol* **15**: 544–550.
1207 Gerken AR, Eller OC, Hahn D a, Morgan TJ. 2015. Constraints, independence, and
1208 evolution of thermal plasticity: Probing genetic architecture of long- and short-
1209 term thermal acclimation. *Proc Natl Acad Sci U S A* **112**: 4399–404.
1210 http://www.ncbi.nlm.nih.gov/pubmed/25805817.
1211 Gnerre S, Maccallum I, Przybylski D, Ribeiro FJ, Burton JN, Walker BJ, Sharpe T, Hall
1212 G, Shea TP, Sykes S, et al. 2011. High-quality draft assemblies of mammalian
1213 genomes from massively parallel sequence data. *Proc Natl Acad Sci U S A* **108**:
1214 1513–1518.

1215 Grabherr MG, Haas BJ, Yassour M, Levin JZ, Thompson D a, Amit I, Adiconis X, Fan L,
1216 Raychowdhury R, Zeng Q, et al. 2011. Full-length transcriptome assembly from
1217 RNA-Seq data without a reference genome. *Nat Biotechnol* **29**: 644–52.
1218 http://www.pubmedcentral.nih.gov/articlerender.fcgi?artid=3571712&tool=pm
1219 centrez&rendertype=abstract (Accessed March 19, 2014).
1220 Guénard B, Weiser MD, Gómez K, Narula N, Economo EP. 2017. The Global Ant
1221 Biodiversity Informatics (GABI) database: Synthesizing data on the geographic
1222 distribution of ant species (Hymenoptera: Formicidae). *Myrmecological News*
1223 **24**: 83–89.
1224 Harpur BA, Kent CF, Molodtsova D, Lebon JMD, Alqarni AS, Owayss AA, Zayed A.
1225 2014. Population genomics of the honey bee reveals strong signatures of
1226 positive selection on worker traits. *Proc Natl Acad Sci* **111**: 2614–2619.
1227 http://www.pnas.org/cgi/doi/10.1073/pnas.1315506111.
1228 Haslbeck M, Vierling E. 2015. A first line of stress defense: Small heat shock proteins
1229 and their function in protein homeostasis. *J Mol Biol* **427**: 1537–1548.
1230 http://dx.doi.org/10.1016/j.jmb.2015.02.002.
1231 Heled J, Drummond AJ. 2010. Bayesian inference of species trees from multilocus
1232 data. *Mol Biol Evol* **27**: 570–80.
1233 http://www.pubmedcentral.nih.gov/articlerender.fcgi?artid=2822290&tool=pm
1234 centrez&rendertype=abstract (Accessed February 29, 2012).
1235 Hess B, Bekker H, Berendsen HJC, Fraaije JGEM. 1997. LINCS: A Linear Constraint
1236 Solver for molecular simulations. *J Comput Chem*.
1237 Hess B, Kutzner C, Van Der Spoel D, Lindahl E. 2008. GRGMACS 4: Algorithms for
1238 highly efficient, load-balanced, and scalable molecular simulation. *J Chem*

1239 *Theory Comput*.

1240 Hijmans RJ, Cameron SE, Parra JL, Jones PG, Jarvis A. 2005. Very high resolution

1241 interpolated climate surfaces for global land areas. *Int J Climatol* **25**: 1965–

1242 1978.

1243 Hoff KJ, Lange S, Lomsadze A, Borodovsky M, Stanke M. 2015. BRAKER1:

1244 Unsupervised RNA-Seq-based genome annotation with GeneMark-ET and

1245 AUGUSTUS. *Bioinformatics* **32**: 767–769.

1246 Hölldobler B, Wilson EO. 1990. *The Ants*.

1247 Holt RD. 2009. Bringing the Hutchinsonian niche into the 21st century: Ecological and

1248 evolutionary perspectives. *Proc Natl Acad Sci* **106**: 19659–19665.

1249 http://www.pnas.org/cgi/doi/10.1073/pnas.0905137106.

1250 Ivens ABF, Kronauer DJC, Pen I, Weissing FJ, Boomsma JJ. 2012. Ants farm

1251 subterranean aphids mostly in single clone groups - An example of prudent

1252 husbandry for carbohydrates and proteins? *BMC Evol Biol* **12**.

1253 Janicki J, Narula N, Ziegler M, Guénard B, Economo EP. 2016. Visualizing and

1254 interacting with large-volume biodiversity data using client-server web-mapping

1255 applications: The design and implementation of antmaps.org. *Ecol Inform* **32**:

1256 185–193.

1257 Jayakumar PC, Shouche YS, Patole MS. 2007. Functional analysis of *Drosophila*

1258 *melanogaster* hexokinase Hex-A locus□: multiple Initiator-like elements

1259 enhance DPE containing promoter activity. **16**: 3–13.

1260 Jorgensen WL, Chandrasekhar J, Madura JD, Impey RW, Klein ML. 1983. Comparison

1261 of simple potential functions for simulating liquid water. *J Chem Phys*.

1262 Kaduk M, Sonnhammer E. 2017. Improved orthology inference with Hieranoid 2.

Bioinformatics **5**: btw774.
http://bioinformatics.oxfordjournals.org/lookup/doi/10.1093/bioinformatics/btw774.

Keeling CI, Yuen MM, Liao NY, Roderick Docking T, Chan SK, Taylor G a, Palmquist DL, Jackman SD, Nguyen A, Li M, et al. 2013. Draft genome of the mountain pine beetle, Dendroctonus ponderosae Hopkins, a major forest pest. *Genome Biol* **14**: R27.
http://www.pubmedcentral.nih.gov/articlerender.fcgi?artid=4053930&tool=pmcentrez&rendertype=abstract.

Kelley JL, Peyton JT, Fiston-Lavier A-S, Teets NM, Yee M-C, Johnston JS, Bustamante CD, Lee RE, Denlinger DL. 2014. Compact genome of the Antarctic midge is likely an adaptation to an extreme environment. *Nat Commun* **5**: 4611.
http://www.nature.com/ncomms/2014/140812/ncomms5611/full/ncomms5611.html.

Körner C, Paulsen J, Spehn EM. 2011. A definition of mountains and their bioclimatic belts for global comparisons of biodiversity data. *Alp Bot* **121**: 73–78.

Kosakovsky Pond SL, Frost SDW, Muse S V. 2005. HyPhy: Hypothesis testing using phylogenies. *Bioinformatics* **21**: 676–679.

Krapf P, Russo L, Arthofer W, Möst M, Steiner FM, Schlick-Steiner BC. 2018. An Alpine ant's behavioural polymorphism: monogyny with and without internest aggression in Tetramorium alpestre. *Ethol Ecol Evol* **30**: 220–234.
https://www.tandfonline.com/doi/full/10.1080/03949370.2017.1343868.

Kuhlemann J. 2007. Paleogeographic and paleotopographic evolution of the Swiss and Eastern Alps since the Oligocene. *Glob Planet Change* **58**: 224–236.

1287 Kumar S, Jones M, Koutsovoulos G, Clarke M, Blaxter M. 2013. Blobology: exploring
1288 raw genome data for contaminants, symbionts and parasites using taxon-
1289 annotated GC-coverage plots. *Front Genet* **4**: 237.
1290 http://www.pubmedcentral.nih.gov/articlerender.fcgi?artid=3843372&tool=pm
1291 centrez&rendertype=abstract.
1292 Lamprecht A, Semenchuk PR, Steinbauer K, Winkler M, Pauli H. 2018. Climate change
1293 leads to accelerated transformation of high-elevation vegetation in the central
1294 Alps. *New Phytol* 447–459. http://doi.wiley.com/10.1111/nph.15290.
1295 Lanfear R, Calcott B, Kainer D, Mayer C, Stamatakis A. 2014. Selecting optimal
1296 partitioning schemes for phylogenomic datasets. *BMC Evol Biol* **14**: 82.
1297 http://www.biomedcentral.com/1471-2148/14/82.
1298 Larkin M a., Blackshields G, Brown NP, Chenna R, Mcgettigan P a., McWilliam H,
1299 Valentin F, Wallace IM, Wilm a., Lopez R, et al. 2007. Clustal W and Clustal X
1300 version 2.0. *Bioinformatics* **23**: 2947–2948.
1301 Levis NA, Pfennig DW. 2016. Evaluating ' Plasticity-First ' Evolution in Nature?: Key
1302 Criteria and Empirical Approaches. *Trends Ecol Evol* **31**: 563–574.
1303 http://dx.doi.org/10.1016/j.tree.2016.03.012.
1304 Librado P, Vieira FG, Rozas J. 2012. BadiRate: Estimating family turnover rates by
1305 likelihood-based methods. *Bioinformatics* **28**: 279–281.
1306 Liu C, Guénard B, Garcia FH, Yamane S, Blanchard B, Yang DR, Economo E. 2015. New
1307 records of ant species from Yunnan, China. *Zookeys* **78**: 17–78.
1308 Liu D, Hu J, Agorreta J, Cesario A, Zhang Y, Harris AL, Gatter K, Pezzella F. 2010a.
1309 Tumor necrosis factor receptor-associated protein 1(TRAP1) regulates genes
1310 involved in cell cycle and metastases. *Cancer Lett* **296**: 194–205.

1311 Liu L, Yu L, Edwards S V. 2010b. A maximum pseudo-likelihood approach for
1312 estimating species trees under the coalescent model. *BMC Evol Biol* **10**: 302.
1313 http://www.biomedcentral.com/1471-
1314 2148/10/302%5Cnhttp://www.pubmedcentral.nih.gov/articlerender.fcgi?artid=
1315 2976751&tool=pmcentrez&rendertype=abstract.
1316 Macdonald HC, Cunha L, Bruford MW, Florestas E, Macdonald HC, Sir T, Evans M,
1317 Avenue M. 2016. Development of genomic resources for four potential
1318 environmental bioindicator species: *Isoperla grammatica*, *Amphinemura*
1319 *sulcicollis*, *Oniscus asellus* and *Baetis rhodani*. *bioRxivorg*.
1320 Marchler-Bauer A, Bo Y, Han L, He J, Lanczycki CJ, Lu S, Chitsaz F, Derbyshire MK,
1321 Geer RC, Gonzales NR, et al. 2017. CDD/SPARCLE: Functional classification of
1322 proteins via subfamily domain architectures. *Nucleic Acids Res* **45**: D200–D203.
1323 Merow C, Smith MJ, Silander JA. 2013. A practical guide to MaxEnt for modeling
1324 species' distributions: What it does, and why inputs and settings matter.
1325 *Ecography (Cop)* **36**: 1058–1069.
1326 Moreau CS, Bell CD. 2013. Testing The Museum Versus Cradle Tropical Biological
1327 Diversity Hypothesis: Phylogeny, Diversification, And Ancestral Biogeographic
1328 Range Evolution Of The Ants. *Evolution (N Y)* **67**: 2240–2257.
1329 Mulichak AM, Wilson JE, Padmanabhan K, Garavito RM. 2002. The structure of
1330 mammalian hexokinase-1. *Nat Struct Biol*.
1331 Nguyen AD, Gotelli NJ, Cahan SH. 2016. The evolution of heat shock protein
1332 sequences, cis-regulatory elements, and expression profiles in the eusocial
1333 Hymenoptera. *BMC Evol Biol* **16**: 15. http://www.biomedcentral.com/1471-
1334 2148/16/15.

1335 Nygaard S, Hu H, Li C, Schiøtt M, Chen Z, Yang Z, Xie Q, Ma C, Deng Y, Dikow R, et al.
1336 2016. Reciprocal genomic evolution in the ant-fungus agricultural symbiosis.
1337 *Nat Commun* 1–9.
1338 Paradis E, Claude J, Strimmer K. 2004. APE: Analyses of phylogenetics and evolution
1339 in R language. *Bioinformatics* **20**: 289–290.
1340 Parker DJ, Wiberg RAW, Trivedi U, Tyukmaeva VI, Gharbi K, Butlin RK, Hoikkala A,
1341 Kankare M, Ritchie MG. 2018. Inter and Intraspecific Genomic Divergence in
1342 Drosophila montana Shows Evidence for Cold Adaptation. **10**: 2086–2101.
1343 Parker J, Tsagkogeorga G, Cotton J a, Liu Y, Provero P, Stupka E, Rossiter SJ. 2013.
1344 Genome-wide signatures of convergent evolution in echolocating mammals.
1345 *Nature* **502**: 1–9.
1346 http://dx.doi.org/10.1038/nature12511%5Cnpapers2://publication/doi/10.103
1347 8/nature12511.
1348 Parrinello M, Rahman A. 1981. Polymorphic transitions in single crystals: A new
1349 molecular dynamics method. *J Appl Phys*.
1350 Peng Y, Leung HCM, Yiu SM, Chin FYL. 2012. IDBA-UD: a *de novo* assembler for
1351 single-cell and metagenomic sequencing data with highly uneven depth.
1352 *Bioinformatics* **28**: 1420–1428.
1353 http://www.ncbi.nlm.nih.gov/pubmed/22495754 (Accessed July 24, 2014).
1354 Prescott SL, Srinivasan R, Marchetto MC, Grishina I, Narvaiza I, Selleri L, Gage FH,
1355 Swigut T, Wysocka J. 2015. Enhancer Divergence and cis-Regulatory Evolution in
1356 the Human and Chimp Neural Crest. *Cell* **163**: 68–84.
1357 Price MN, Dehal PS, Arkin AP. 2010. FastTree 2 - Approximately maximum-likelihood
1358 trees for large alignments. *PLoS One* **5**: e9490.

1359 Pringle EG, Novo A, Ableson I, Barbehenn R V, Vannette RL. 2014. Plant-derived
1360 differences in the composition of aphid honeydew and their effects on colonies
1361 of aphid-tending ants.
1362 Ranwez V, Harispe S, Delsuc F, Douzery EJP. 2011. MACSE: Multiple alignment of
1363 coding SEquences accounting for frameshifts and stop codons. *PLoS One* **6**:
1364 e22594.
1365 Rogora M, Frate L, Carranza ML, Freppaz M, Stanisci A, Bertani I, Bottarin R,
1366 Brambilla A, Canullo R, Carbognani M, et al. 2018. Assessment of climate
1367 change effects on mountain ecosystems through a cross-site analysis in the Alps
1368 and Apennines. *Sci Total Environ* **624**: 1429–1442.
1369 https://doi.org/10.1016/j.scitotenv.2017.12.155.
1370 Roux J, Privman E, Moretti S, Daub JT, Robinson-Rechavi M, Keller L. 2014. Patterns
1371 of positive selection in seven ant genomes. *Mol Biol Evol* **31**: 1661–1685.
1372 Sanderson MJ. 2002. Estimating absolute rates of molecular evolution and
1373 divergence times: a penalized likelihood approach. *Mol Biol Evol* **19**: 101–109.
1374 http://www.ncbi.nlm.nih.gov/pubmed/11752195.
1375 Seifert B. 2018. *The ants of Central and North Europe*. ed. Tauer. Lutra Verlags- und
1376 Vertriebsgesellschaft.
1377 Shaw TI, Ruan Z, Glenn TC, Liu L. 2013. STRAW: Species TRee Analysis Web server.
1378 *Nucleic Acids Res* **41**: 238–241.
1379 Sillitoe I, Lewis TE, Cuff A, Das S, Ashford P, Dawson NL, Furnham N, Laskowski RA,
1380 Lee D, Lees JG, et al. 2015. CATH: Comprehensive structural and functional
1381 annotations for genome sequences. *Nucleic Acids Res* **43**: D376–D381.
1382 Simão FA, Waterhouse RM, Ioannidis P, Kriventseva E V., Zdobnov EM. 2015. BUSCO:

1383 Assessing genome assembly and annotation completeness with single-copy
1384 orthologs. *Bioinformatics* **31**: 3210–3212.
1385 Slater GSC, Birney E. 2005. Automated generation of heuristics for biological
1386 sequence comparison. *BMC Bioinformatics* **6**: 1–11.
1387 Smit A, Hubley R, Green P. 2013. RepeatMasker Open-4.0. 2013-2015 .
1388 *http://www.repeatmasker.org*. http://repeatmasker.org.
1389 Soberón J. 2007. Grinnellian and Eltonian niches and geographic distributions of
1390 species. *Ecol Lett* **10**: 1115–1123.
1391 Sonnhammer ELL, Östlund G. 2015. InParanoid 8: Orthology analysis between 273
1392 proteomes, mostly eukaryotic. *Nucleic Acids Res* **43**: D234–D239.
1393 Sousa Da Silva AW, Vranken WF. 2012. ACPYPE - AnteChamber PYthon Parser
1394 interfacE. *BMC Res Notes*.
1395 Stanke M, Schöffmann O, Morgenstern B, Waack S. 2006. Gene prediction in
1396 eukaryotes with a generalized hidden Markov model that uses hints from
1397 external sources. *BMC Bioinformatics* **7**: 62.
1398 Steiner FM, Seifert B, Moder K, Schlick-Steiner BC. 2010. A multisource solution for a
1399 complex problem in biodiversity research: Description of the cryptic ant species
1400 Tetramorium alpestre sp.n. (Hymenoptera: Formicidae). *Zool Anzeiger - A J*
1401 *Comp Zool* **249**: 223–254.
1402 http://linkinghub.elsevier.com/retrieve/pii/S0044523110000537 (Accessed
1403 April 9, 2014).
1404 Trapnell C, Roberts A, Goff L, Pertea G, Kim D, Kelley DR, Pimentel H, Salzberg SL,
1405 Rinn JL, Pachter L. 2012. Differential gene and transcript expression analysis of
1406 RNA-seq experiments with TopHat and Cufflinks. *Nat Protoc* **7**: 562–578.

1407 http://www.nature.com/doifinder/10.1038/nprot.2012.016 (Accessed March 1,
1408 2012).
1409 Uchida Y, Uesaka M, Yamamoto T, Takeda H, Irie N. 2018. Embryonic lethality is not
1410 sufficient to explain hourglass-like conservation of vertebrate embryos. *Evodevo*
1411 **9**: 1–11. https://doi.org/10.1186/s13227-018-0095-0.
1412 Wagner GP, Lynch VJ. 2010. Evolutionary novelties. *Curr Biol* **20**: 48–52.
1413 https://pdf.sciencedirectassets.com/272099/1-s2.0-S0960982210X00021/1-
1414 s2.0-S0960982209019459/main.pdf?x-amz-security-
1415 token=AgoJb3JpZ2luX2VjECIaCXVzLWVhc3QtMSJHMEUCIDsUh2jRKJL1EeOiMrN
1416 glWa%2BljWFLis7tEu%2FF65JtK%2FrAiEA3Ge%2FEhYUyff41n0NLuT%2F6f3OMY
1417 i9qUIAiE.
1418 Wagner HC, Arthofer W, Seifert B, Muster C, Steiner FM, Schlick-Steiner BC. 2017.
1419 Light at the end of the tunnel: Integrative taxonomy delimits cryptic species in
1420 the Tetramorium caespitum complex (Hymenoptera: Formicidae).
1421 *Myrmecological News* **25**: 95–129.
1422 Wallis GP, Waters JM, Upton P, Craw D. 2016. Transverse Alpine Speciation Driven by
1423 Glaciation. *Trends Ecol Evol* **31**: 916–926.
1424 http://dx.doi.org/10.1016/j.tree.2016.08.009.
1425 Warde-Farley D, Donaldson SL, Comes O, Zuberi K, Badrawi R, Chao P, Franz M,
1426 Grouios C, Kazi F, Lopes CT, et al. 2010. The GeneMANIA prediction server:
1427 biological network integration for gene prioritization and predicting gene
1428 function eds. J. Weaver, K. Anija, and T. Daspit. *Nucleic Acids Res* **38**: W214–
1429 W220. http://nar.oxfordjournals.org/content/38/suppl_2/W214.short
1430 (Accessed March 1, 2013).

1431 Webb B, Sali A. 2014. Protein structure modeling with MODELLER. *Methods Mol Biol*
1432 **1137**: 1–15.
1433 http://www.springerlink.com/openurl.asp?genre=book&id=doi:10.1385/15925
1434 93682%5Cnhttp://link.springer.com/10.1007/978-1-4939-0366-
1435 5%5Cnhttp://link.springer.com/protocol/10.1007/978-1-60327-058-
1436 8_8%5Cnhttp://www.ncbi.nlm.nih.gov/pubmed/24573470.
1437 Wertheim JO, Murrell B, Smith MD, Kosakovsky Pond SL, Scheffler K. 2014. RELAX:
1438 Detecting relaxed selection in a phylogenetic framework. *Mol Biol Evol* **32**: 1–
1439 13. http://www.ncbi.nlm.nih.gov/pubmed/25540451.
1440 Wilson EO. 1990. *Success and Dominance in Ecosystems: The Case of Social Insects*.
1441 Xian-Wu L, Wei-Hua X. 2016. Hexokinase is a key regulator of energy metabolism and
1442 ROS activity in insect lifespan extension. *Aging (Albany NY)* **8**: 245–258.
1443 https://www.ncbi.nlm.nih.gov/pmc/articles/PMC4789580/pdf/aging-08-
1444 245.pdf.
1445 Yoshida S, Tsutsumi S, Muhlebach G, Sourbier C, Lee M-J, Lee S, Vartholomaiou E,
1446 Tatokoro M, Beebe K, Miyajima N, et al. 2013. Molecular chaperone TRAP1
1447 regulates a metabolic switch between mitochondrial respiration and aerobic
1448 glycolysis. *Proc Natl Acad Sci* **110**: E1604–E1612.
1449 http://www.pnas.org/cgi/doi/10.1073/pnas.1220659110.
1450 Zachos J, Pagani M, Sloan L, Thomas E, Billups K. 2001. Trends, Rythms, and
1451 Aberration in Global Climate 65 Ma to Present. *Science (80-)* **292**: 686–693.
1452